Chaos
An Interdisciplinary Journal of Nonlinear Science

RESEARCH ARTICLE | OCTOBER 11 2023

Impact of Allee and fear effects in a fractional order prey–predator system with group defense and prey refuge

Wenhui Tan ; Hao Tian; Yanjie Song ; Xiaojun Duan

Chaos 33, 103113 (2023)
https://doi.org/10.1063/5.0157354

Impact of Allee and fear effects in a fractional order prey–predator system with group defense and prey refuge

Cite as: Chaos 33, 103113 (2023); doi: 10.1063/5.0157354
Submitted: 7 May 2023 · Accepted: 13 September 2023 ·
Published Online: 11 October 2023

Wenhui Tan,[1,a)] Hao Tian,[2] Yanjie Song,[3] and Xiaojun Duan[1]

AFFILIATIONS

[1]College of Science, National University of Defense Technology, Changsha, Hunan 410073, China
[2]College of Science, China Agricultural University, Beijing 100864, China
[3]College of Management and Economics, Tianjin University, Tianjin 300072, China

Note: This paper is part of the Focus Issue on Nonlinear Model Reduction From Equations and Data.
[a)]**Author to whom correspondence should be addressed:** tanwenhui0@163.com

ABSTRACT

This paper presents a novel fractional-order model of a prey–predator system that incorporates group defense and prey refuge mechanisms, along with Allee and fear effects. First, we examine the existence, uniqueness, non-negativity, and boundedness of the solution of the system. Second, a comprehensive analysis is conducted on the existence, stability, and coexistence of equilibrium states in the system, which are crucial for comprehending prey–predator system behavior. Our investigation reveals that the coexistence equilibrium undergoes a Hopf bifurcation under five key parameters. Specifically, an increased threshold for the transition between group and individual behavior, influenced by different strengths of the Allee effect, enhances the stability of both populations. This discovery sheds light on the role of group effects in shaping prey–predator interactions and ecosystem stability. Third, system discretization is employed to explore the impact of step size on stimulating stability and to investigate the Neimark–Sacker bifurcation, providing a more comprehensive understanding of system behavior. The role of step size as a constraint on stability is examined, revealing the system's progression from stability to chaos. Consequently, our results offer a more flexible mechanism for adjusting the stability and dynamics of the two species. Finally, numerical simulations are utilized to validate the reasonableness of the research findings.

This paper introduces a novel fractional-order prey–predator system that includes group defense, prey refuge, Allee effect, and fear effect and provides a more flexible scheme for regulating the two species' stable coexistence and dynamical mechanisms. It offers valuable insights into the various factors influencing the system's dynamics. First, the strength of the Allee effect has diverse impacts on the number, stability, and bifurcation of equilibrium points. For instance, under the strong Allee effect, the system manifests an extinction equilibrium, two prey-only equilibria, and one coexistence equilibrium. As the strength of the Allee effect increases, the area of initial density attracted to the locally progressively stable extinction equilibrium also increases, thereby posing a greater risk of extinction for both population systems. However, as the Allee effect weakens, one of the moving boundary equilibria vanishes, and the extinction equilibrium becomes a saddle point. It is noteworthy that prey populations remain viable irrespective of the initial density of the two populations. Second, when Hopf bifurcation occurs at the coexistence equilibrium, an appropriate reduction of the Allee effect, prey population mortality, memory effect, or an increase of transition thresholds between group and solidarity behavior, predator numbers, and prey conservation effects can stabilize grouping and solitariness in the two populations. The study emphasizes that increasing thresholds for transitions between group grouping and solitary behavior, memory effect, and reducing memory effects are crucial for maintaining population equilibrium. Third, fractional-order continuous systems pose challenges in numerical simulations; thus, discrete systems are employed to comprehensively understand the process from bifurcation to the emergence of singular attractors. This paper discretizes the system and demonstrates that equilibrium stability changes when step size thresholds are exceeded, leading to more complex systems, such as generating

chaos through Neimark–Sacker bifurcation. Selecting an appropriate step size is critical to facilitating species coexistence, and adjusting the step size according to the fractional order is more conducive to capturing the complexity of both populations. The outcomes of this study have significant implications for comprehending prey–predator interactions and ecosystem stability.

I. INTRODUCTION

Prey–predator models have been extensively studied in the fields of biology and mathematics[1–3] since the seminal works of Lotka[4] and Volterra.[5] Understanding the dynamics of prey–predator interactions, including stability, persistence, periodic solutions, and bifurcation, is crucial for maintaining the balance of ecosystems.[6–8] A variety of functional response functions, such as Holling–Tanner, ratio-dependent, and Beddington–DeAngelis types, have been proposed to describe the interaction between predator and prey populations.[9–16] To better understand the intricate dynamics of prey–predator interactions, applied mathematicians and theoretical ecologists have incorporated several ecological phenomena into their models, including the Allee effect, the fear effect, the nonlocal competition effect, and the environmental impact.[17–28]

In natural ecosystems, many species exhibit social behavior that can influence the behavior of other members of their population. For example, species, such as wildebeest, zebras, and buffalo, form herds to search for food resources or defend against predators. This herd behavior can provide a strong selective advantage, contributing to the long-term success of a population or ecosystem. Recently, a prey–predator model has been studied in which the prey exhibits herd behavior, and the predator interacts with the prey along the outer corridor of the herd of prey. It has been suggested that the response functions of prey that exhibit herd behavior should be modeled in terms of the square root of the prey population.[29–31] This approach could improve the accuracy of prey–predator models that take into account social behavior. Based on this fact, the authors in Ref. 32 have proposed a prey–predator model described by the following ordinary differential equations:

$$\begin{cases} \dfrac{du}{dt} = u(1-u) - \sqrt{u}v, \\ \dfrac{dv}{dt} = \tilde{\gamma} v(-\tilde{\beta} + \sqrt{u}), \end{cases}$$

where $u(t)$ and $v(t)$ stand for the prey and predator densities at time t, respectively. $\tilde{\beta}\tilde{\gamma}$ is the death rate of the predator in the absence of prey, and $\tilde{\gamma}$ is the conversion or consumption rate of prey to predator.

It is essential to consider the size of the herd in the effectiveness of herd behavior as a protective measure for prey populations against predators. When the herd is too small, it may not be able to provide an adequate group defense as the boundary of the herd may consist of the total population, making it easier for predators to attack. The authors in Ref. 33 studied a modified prey–predator model incorporating herd behavior to address this. The model is described as

$$\begin{cases} \dfrac{du}{dt} = ru\left(1 - \dfrac{u}{K}\right) - a\dfrac{u}{\sqrt{u+h}}v, \\ \dfrac{dv}{dt} = -mv + ea\dfrac{u}{\sqrt{u+h}}v, \end{cases}$$

where r is the intrinsic growth rates of the prey, K is the carrying capacity of the prey, a is the maximum value of prey consumed by per predator per unit time, h is a threshold for the transition between herd grouping and solitary behavior, m is the death rate of the predator in the absence of prey, and e is the conversion or consumption rate of prey to predator. This model provides a useful framework for studying the dynamics of prey–predator interactions in the presence of herd behavior.

For many years, the conventional view in ecology was that predators only influence prey population sizes through direct predation. However, recent research has shown that predators can also impact prey behavior and physiology, resulting in changes in prey population dynamics.[34,35] These indirect effects may be even more significant than direct predation. Prey animals can display a range of anti-predator responses, including changes in habitat use, foraging behavior, vigilance, and physiological changes. Incorporating predator call playback into a prey–predator model, the authors in Ref. 36 explored the impact of fear-induced changes in behavior on prey–predator dynamics. They found that isolation can mitigate the effects of direct predation, as prey animals become less vulnerable when separated from other members of the population. These findings underscore the complex interplay between social behavior, prey–predator dynamics, and fear effects. Real-world experiments have demonstrated that predation risk can have a significant impact on wildlife populations, with some studies showing up to a 40% decrease in sparrow offspring numbers due to fear-induced behavioral changes. The authors in Ref. 37 found that the stability of the positive equilibrium point changes from stable to unstable and then back to stable with an increase in the fear effect. Currently, the system can be in a stable state at very low or high levels of the fear effect, with two nearby Hopf branches near the positive equilibrium point for the fear coefficient.

It is known that the Allee effect, introduced by well known ecologist W. C. Allee, is an important mechanism in ecology which gives realistic description of interaction among species in ecosystem. It refers to a positive relationship between the population density and per capita growth rate of the population at small densities. In recent years, intense focus has been given to studying these phenomena on prey–predator models not only in ecology but also in other disciplines.[38–40] The Allee effect deals with the extinction scenario of the species in which there is some critical density of the population, called Allee threshold, which influences the extinction. Allee effects can be classified into two types: strong Allee effect and weak Allee effect. In the case of a strong Allee effect, the per capita growth rate is negative below the Allee threshold and the growth rate becomes positive above that threshold. In the case of a weak Allee effect, the per capita growth rate is small but remains positive at low population densities. Compared to a strong Allee effect, no critical density is required for survival of the population in the case of a weak Allee effect.[41] The Allee effect can be induced by a variety of mechanisms,

TABLE I. Biological significance description of parameters in system (1.2).

Parameter	Meaning
$u(t)$	Prey population density at time t
$v(t)$	Predator population density at time t
$m \in (-1, 1)$	Allee effect
$k > 0$	The level of fear effect
$a > 0$	The maximum value of prey consumed by per predator per unit time
$u(1-e)$	Amount of the prey available to the predator
$h \in (0, 1)$	Threshold for the transition between herd grouping and solitary behavior
b/a	Conversion rate of the prey
$d > 0$	Death rate of the predator population
$q, 1 \geq q > 0$	The order of fractional-order differential equation of the system

including difficulties in finding suitable mating partners, reproductive facilitation and predation, social interaction, pollen scarcity and anti-predator behavior, and environmental conditioning.[42–45] The Allee effect is a crucial mechanism in ecology that provides a realistic description of interactions among species in ecosystems. The effect refers to the positive relationship between population density and per capita growth rate at low densities. Recent studies have focused on applying the Allee effect to prey–predator models in ecology and other disciplines. The effect is classified into two types: strong Allee effect and weak Allee effect, depending on whether or not a critical population density is needed for the population's survival. Various mechanisms can induce the Allee effect, including difficulties in finding suitable mating partners, reproductive facilitation, predation, social interaction, pollen scarcity, anti-predator behavior, and environmental conditioning. The authors in Ref. 46 studied the dynamic behaviors of a fractional-order prey–predator system incorporating the Allee effect, fear effect, and shelter effect. They found that stable coexistence could be achieved by appropriately increasing the fear level or refuge rate or reducing prey natality or the fractional order of the system. Motivated by previous studies, the following prey–predator system with Allee and fear effects in the prey is put forward,

$$\begin{cases} \dfrac{du}{dt} = \dfrac{u(1-u)(u-m)}{1+kv} - \dfrac{a(1-e)uv}{\sqrt{u(1-e)+h}}, \\ \dfrac{du}{dt} = \dfrac{b(1-e)uv}{\sqrt{u(1-e)+h}} - dv. \end{cases}$$

The meanings of all parameters of system (1.2) are presented in Table I.

Over the past two decades, researchers have focused on investigating the dynamic behavior of fractional ecosystems, as fractional calculus has the ability to represent the memory and genetic effects of species in most ecosystems throughout their entire lifespan.[47,48] The authors in Ref. 49 studied three species fractional food web models within the framework of the improved Caputo–Fabrizio operator, the system's complexity was observed through simulations of various fractional orders and initial values. Studies in this area have explored the existence and uniqueness of system solutions, stability of system equilibrium points, and Hopf bifurcation of systems, among other topics. Building on this previous research, this study aims to investigate how Allee, fear, and refuge effects impact the dynamics of the prey–predator system under the fractional prey–predator system. To achieve this goal, the Caputo fractional differential equation is employed to describe the memory effect of the population, and a new prey–predator fractional system is proposed, which incorporates Allee and fear effects with group defense and prey refuge. The system can be expressed as follows:

$$\begin{cases} \dfrac{du}{dt} = \int_{t_0}^{t} \nu\,(t-t') \left(\frac{u(1-u)(u-m)}{1+kv} - \frac{a(1-e)v}{\sqrt{u(1-e)+h}} \right) dt', \\ \dfrac{dv}{dt} = \int_{t_0}^{t} \nu\,(t-t') \left(\frac{b(1-e)uv}{\sqrt{u(1-e)+h}} - dv \right) dt', \end{cases} \tag{1.1}$$

where $\nu(t-t') = \frac{1}{\Gamma(q-1)}(t-t')^{q-2}$ and $\Gamma(x)$ denotes the gamma function. The coefficient $1/\Gamma(q-1)$ and exponent $(q-2)$ are chosen to rewrite Eq. (1.1) in the form of fractional differential equations with the Caputo-type derivative. By applying the Caputo fractional derivative of $(q-1)$ on both sides and using the fact that the Caputo fractional derivative and the fractional integral are inverse operations, the following fractional differential equation can be obtained:

$$\begin{cases} {}_0^C D_t^q u(t) = \dfrac{u(1-u)(u-m)}{1+kv} - \dfrac{a(1-e)uv}{\sqrt{u(1-e)+h}}, \\ {}_0^C D_t^q v(t) = \dfrac{b(1-e)uv}{\sqrt{u(1-e)+h}} - dv. \end{cases} \tag{1.2}$$

The meanings of all parameters of system (1.2) are presented in Table I.

Three main contributions are presented in this paper.

(1) This paper proposes a new fractional-order system containing group defense, prey refuge, Allee and fear effects.
(2) Since multiple effects, especially the Allee, group, and memory effects, have a significant impact on biological games, this paper focuses on five critical parameters and the mechanism of the memory effect on the stability of prey–predator and Hopf bifurcation. Extensive theoretical and numerical analyses show the system's equilibrium under different parameters.
(3) To reveal the effect of step length on prey–predator stability and bifurcation, we explore the constraint of step length on equilibrium by discretizing system (1.2) while keeping the number of equilibria constant and showing the process of the system from stability to chaos. It provides a more flexible scheme for regulating the stable coexistence and dynamics of the two species and provides valuable insights into the various factors that influence the system's dynamics.

This paper is organized as follows: Sec. II provides some fractional-order theoretical knowledge for later use. Section III studies the existence of uniqueness, non-negativity, and boundedness of the system in a fractional-order framework. Section IV investigates the existence of equilibrium points of the system and integrates the local and global stability of the equilibrium points of the system

and Hopf bifurcation. Section V investigates the system's stability after discretization with Neimark–Sacker bifurcation. This study is essential to assess the effect of discretization on the system's stability. Section VI verifies the soundness of the obtained results by numerical simulations. Finally, Sec. VII presents a short conclusion.

II. PRELIMINARIES

In this section, we discuss some crucial definitions, useful lemmas, and theorems related to fractional calculus.

Definition 1 (Ref. 50): *The Caputo fractional derivative with order $q \geq 0$ for the continuous function $g(t) \in \mathcal{AC}^n([0,+\infty),\mathbb{R})$ is defined as*

$$ {}_0^C D_t^q g(t) = \frac{1}{\Gamma(n-q)} \int_0^t \frac{g^{(n)}(s)}{(t-s)^{q-n+1}} ds, $$

where $q \in (n-1, n)$ and $n \in \mathbb{Z}_+$, $\Gamma(\cdot)$ is the Gamma function.

In particular, when $n = 1$, i.e., $0 < q \leq 1$, the Caputo fractional derivative with order q becomes

$$ {}_0^C D_t^q g(t) = \frac{1}{\Gamma(1-q)} \int_0^t \frac{g(s)}{(t-s)^q} ds. $$

Definition 2 (Ref. 50): *The Mittag–Leffler function E_l for order $l > 0$ is defined as*

$$ E_l(z) := \sum_{j=0}^{\infty} \frac{z^j}{\Gamma(jl+1)}, \quad z \in \mathbb{C} $$

as the sequence converges.

Lemma 1 (Ref. 51): *For system*

$$ {}_0^C D_t^q X(t) = \Psi(t, X), t \geq 0, $$

with initial condition $X(0) = (x(0), y(0))$, where $0 < q \leq 1$, $\Psi : [0,\infty) \times \Delta \to \mathbb{R}_n$, $\Delta \subseteq \mathbb{R}_n$, if $\Psi(t, X)$ fulfills the local Lipschitz condition about $X \in \mathbb{R}_n$,

$$ \|\Psi(t, X) - \Psi(t, \tilde{X})\| \leq M\|X - \tilde{X}\|, $$

then the system exists a unique solution on $[0,\infty) \times \Delta$, and $\left\|X(x_1, x_2, \ldots, x_n) - \tilde{X}(\tilde{x}_1, \tilde{x}_2, \ldots, \tilde{x}_n)\right\| \leq \sum_{i=1}^n |x_i - \tilde{x}_i|$, $i = 1, 2, \ldots, n, x_i, \tilde{x}_i \in \mathbb{R}$.

Theorem 1 (Ref. 52): *The Laplace transform of ${}_0^C D_t^q g(t)$ is*

$$ \mathscr{L}\left\{{}_0^C D_t^q g(t)\right\} = s^q F(s) - \sum_{i=0}^{n-1} s^{q-i-1} g^i(0), $$

where $F(s) = \mathscr{L}\{g(t)\}$, $q \in (n-1, n)$ and $n \in \mathbb{Z}_+$.

Theorem 2 (Ref. 53): *Assume $q > 0$, $\beta > 0$, and $K \in \mathbb{C}^{n\times n}$, then*

$$ \mathscr{L}\left\{t^{\beta-1} E_{q,\beta}(Kt^q)\right\} = \frac{s^{q-\beta}}{s^q - K} $$

for $\mathrm{Re}(s) > \|K\|^{\frac{1}{q}}$, where $\mathrm{Re}(s)$ is the real part of the complex number s and $E_{q,\beta}$ is the Mittag–Leffler function.

Theorem 3 (Ref. 54): *For the following fractional-order system:*

$$ {}_0^C D_t^q g(t) = h(g(t)), \quad g(0) = g_0 \in \mathbb{R}^N, \quad q \in (0,1), $$

where $g(t) = (g_1(t), g_2(t), \ldots, g_n(t))^T \in \mathbb{R}^n$ and $h : [h_1, h_2, \ldots, h_n]: \mathbb{R}^n \to \mathbb{R}^n$. If $h(g^*) = 0$, then g^* is an equilibrium point. Set $J(g^*)$ is the Jacobian matrix $J = \frac{\partial h}{\partial g} = \frac{\partial(h_1, h_2, \ldots, h_n)}{\partial(g_1, g_2, \ldots, g_n)}$ for $g = g^*$. If the characteristic values $\lambda_i (i = 1, \ldots, n)$ of $J(g^*)$ meet $\left|\arg(\lambda_i)\right| > \frac{q\pi}{2}$ $(i = 1, \ldots, n)$, then g^* is locally asymptotically stable.

Definition 3 (Ref. 55): *A fixed point (x, y) is called*

(i) *sink if $|\lambda_1| < 1$ and $|\lambda_2| < 1$, and it is locally asymptotically stable;*
(ii) *source if $|\lambda_1| > 1$ and $|\lambda_2| > 1$, and it is locally unstable;*
(iii) *saddle if $|\lambda_1| > 1$ and $|\lambda_2| < 1$ or ($|\lambda_1| < 1$ and $|\lambda_2| > 1$); and*
(iv) *non-hyperbolic if either $|\lambda_1| = 1$ or $|\lambda_2| = 1$.*

Lemma 2 (Ref. 56): *Let $F(\lambda) = \lambda^2 + P\lambda + Q$, suppose that $F(1) > 0, \lambda_1$ and λ_2 are two roots of $F(\lambda) = 0$, then*

(i) *$|\lambda_1| < 1$ and $|\lambda_2| < 1$ if and only if $F(-1) > 0$ and $Q < 1$;*
(ii) *$|\lambda_1| < 1$ and $|\lambda_2| > 1$ (or $|\lambda_1| > 1$ and $|\lambda_2| < 1$) if and only if $F(-1) < 0$;*
(iii) *$|\lambda_1| > 1$ and $|\lambda_2| > 1$ if and only if $F(-1) > 0$ and $Q > 1$;*
(iv) *$\lambda_1 = -1$ and $|\lambda_2| \neq 1$ if and only if $F(-1) = 0$ and $P \neq 0, 2$; and*
(v) *λ_1 and λ_2 are complex and $|\lambda_1| = 1, |\lambda_2| = 1$ if and only if $P^2 - 4Q < 0$ and $Q = 1$.*

III. ANALYSIS OF WELL-POSEDNESS OF THE SYSTEM

In this section, we examine the existence, uniqueness, non-negativity, and boundedness of the solutions of system (1.2).

A. Existence and uniqueness of the solutions

Theorem 4: *System (1.2) owns a unique solution $X(t) = (u(t), v(t)) \in \Omega$ with initial condition $(u(0), v(0)) \in \Omega, \forall t \geq 0$.*

Proof. First, we consider the time interval $[0, t_1], t_1 < +\infty$ and the region as follows:

$$ \Omega = \{(u, v) : \max\{|u|, |v|\} < \eta\}, $$

where η is a positive real number and is a subset of $\mathbb{R}^2$, and we choose two points from the set, $\mathbf{X_0}, \tilde{\mathbf{X}}_\mathbf{0} \in \Omega$. Two solutions of the system ${}_0^C D^q \mathbf{X} = \mathbf{F}(\mathbf{X})$, starting from $\mathbf{X_0}$ and $\tilde{\mathbf{X}}_\mathbf{0}$, are denoted by $\mathbf{X}(t)$ and $\tilde{\mathbf{X}}(t)$, respectively. $\mathbf{F}(\mathbf{X}) = (F_1(\mathbf{X}), F_2(\mathbf{X}))$, where $\mathbf{X} = (u, v)^T$ and

$$ \begin{cases} F_1(\mathbf{X}) = \dfrac{u(1-u)(u-m)}{1+kv} - \dfrac{a(1-e)uv}{\sqrt{u(1-e)+h}}, \\ F_2(\mathbf{X}) = \dfrac{b(1-e)uv}{\sqrt{u(1-e)+h}} - dv. \end{cases} $$

Now, we can write

$$\begin{aligned}\|\mathbf{F}(\mathbf{X})-\mathbf{F}(\tilde{\mathbf{X}})\| &= \left|F_1(\mathbf{X})-F_2(\tilde{\mathbf{X}})\right|+\left|F_1(\mathbf{X})-F_2(\tilde{\mathbf{X}})\right| \\ &\leqslant |u-\tilde{u}|\left|(1+k\eta)+\eta^2\right|+2\eta(1+m)|u-\tilde{u}|-m|u-\tilde{u}|+km\eta|v-\tilde{v}|+\frac{1-e}{h}|v-\tilde{v}|\left|a\eta\sqrt{h}+b\eta\sqrt{\eta(1-e)+h}\right| \\ &\leqslant |u-\tilde{u}|\left|(1+k\eta)3\eta^2+2\eta(1+m)-m)\right|+|v-\tilde{v}|\left|km\eta+\frac{1-e}{h}(a\eta\sqrt{h}+b\eta\sqrt{h(-e)+h})\right| \\ &\leqslant L_1|u-\tilde{u}|+L_2|v-\tilde{v}| \\ &\leqslant L\|\mathbf{X}-\tilde{\mathbf{X}}\|,\end{aligned}$$

where $L=\max\{L_1,L_2\}$, $L_1=(1+k\eta)3\eta^2+2\eta(1+m)-m)$, and $L_2=km\eta+\frac{1-e}{h}(a\eta\sqrt{h}+b\eta\sqrt{h(-e)+h})$.

Hence, $\mathbf{F}(\mathbf{X})$ conforms to the condition of local Lipschitz, then system (1.2) exists a unique solution by Lemma 1. □

B. Non-negativity and boundedness of the solutions

Theorem 5: *All solutions of system (1.2) initiating from* $(u(0),v(0))\in R^2$ *are non-negative and bounded in region* $\mathscr{W}$.

Proof. We aim to establish the non-negativity of solutions $u(t)$ that originate from $\mathscr{W}$. In other words, we seek to prove that $u(t)\geq 0$ holds for all $t\geq t_0$. Assuming the contrary, there exists a constant $t_1>t_0$ such that $t_1^+>t_1$ is sufficiently close to t_1, and the following conditions hold:

$$\begin{cases}u(t)>0, t_0\leq t\leq t_1,\\ u(t_1)=0,\\ u\left(t_1^+\right)<0.\end{cases}$$

There are two possibilities:

1. If ${}_0^C D^q u(t)\geq 0$ for all $t\in\left[t_1,t_1^+\right]$, according to Theorem 1 in Ref. 51, it can be concluded that $u(t)$ is a non-decreasing function for each $t\in\left[t_1,t_1^+\right]$. However, this contradicts the initial assumption.
2. If ${}_0^C D^q u(t)\leq 0$ for all $t\in\left[t_1,t_1^+\right]$, we have the inequality

$$\begin{aligned}{}_0^C D_t^q u(t) &\geqslant u\left(\frac{(1-u)(u-m)}{1+k\eta}-\frac{a(1-e)\eta}{\sqrt{u(1-e)+h}}\right) \\ &\geqslant u\max\left(\frac{(1-u)(u-m)}{1+k\eta}-\frac{a(1-e)\eta}{\sqrt{u(1-e)+h}}\right).\end{aligned}$$

Since $u(t)$ is continuous, it attains a minimum value for all $t\in\left[t_1,t_1^+\right]$. Let γ be the maximum value of $\frac{(1-u)(u-m)}{1+k\eta}-\frac{a(1-e)\eta}{\sqrt{u(1-e)+h}}$. Therefore, we have the inequality

$${}_0^C D^q u(t)\geqslant u(t)\gamma.$$

By applying the Laplace transform to this inequality, we obtain

$$u(t)\geqslant u(t_1)E_q\left(\gamma(t-t_1)^q\right), t\in\left[t_1,t_1^+\right].$$

Thus, $u(t)\geqslant 0$ for any $t\geqslant t_1$, which contradicts the assumption. In the same manner, we have $v(t)$ is non-negative.

To prove the boundedness of the solutions of system (1.2), we consider:

$$U(t)=u(t)+\frac{a}{b}v(t).$$

Then, the Caputo fractional derivative of $U(t)$ with order q is

$${}_0^C D_t^q U(t)=\frac{u(1-u)(u-m)}{1+kv}-d\left(U(t)-u\right).$$

Foe any $d>0$, we have

$$\begin{aligned}{}_0^C D_t^q U(t)+dU(t) &= \frac{u(1-u)(u-m)}{1+kv}+du \\ &\leqslant u(1-u)(u-m)+du \\ &\leqslant (d-m)u+(1-m)u^2 \\ &\leqslant 1+d.\end{aligned}$$

Applying Theorems 1 and 2, we obtain $s^qF(s)-s^{q-1}U(0)+dF(s)\leqslant\frac{1+d}{s}$, where $F(s)=\mathcal{L}\{U(t)\}$, i.e.,

$$F(s)\leqslant U(0)\frac{s^{q-1}}{s^q+d}+\frac{1+d}{s\left(s^q+d\right)}.$$

Hence,

$$U(t)\leqslant U(0)E_{q,1}\left\{-dt^q\right\}+(1+d)t^qE_{q,q+1}\left\{-dt^q\right\}.$$

Considering the properties of the Mittag–Leffer function, we have

$$E_{q,1}\left\{-dt^q\right\}=\left(-dt^q\right)E_{q,q+1}\left\{-dt^q\right\}+\frac{1}{F(1)},$$

i.e., $t^qE_{q,q+1}\left\{-dt^q\right\}=-\frac{1}{d}\left(E_{q,1}\left\{-dt^q\right\}-1\right)$ and

$$U(t)\leqslant\left(U(0)-\frac{1+d}{d}\right)E_{q,1}\left\{-dt^q\right\}+\frac{1+d}{d}.$$

Due to the positiveness of the Mittag–Leffler function $E_{q,1}$ and taking the limit $t\to\infty$, we have

$$\lim_{t\to\infty}U(t)\leqslant\frac{1+d}{d}+\varepsilon.$$

Thus, all solutions of system (1.2) are bounded in the region

$$\mathscr{W}=\left\{(u(t),v(t))\in R_+^2\mid 0\leqslant u(t)+\frac{a}{b}v(t)\leqslant\frac{1+d}{d}+\varepsilon,\varepsilon>0\right\}.$$

□

IV. QUALITATIVE ANALYSIS

The main aim of this section is to examine the dynamic behavior of system (1.2) by analyzing its equilibrium points. This investigation focuses on identifying the conditions for the existence and coexistence of equilibrium points and establishing their local and global asymptotic stability. The occurrence of bifurcation at these equilibrium points is thoroughly explored, with particular attention given to Hopf bifurcations induced by parameter variations. The obtained results yield valuable insights into the long-term dynamics of the system and its sensitivity to changes in key parameters.

A. Existence of equilibrium point of system (1.2)

Considering the biological significance of the system, we assume that $m \in (-1,1), a, e, h, d \in (0,1), b \in (a,1), k \in R^+$, then the analysis of the existence of the biological equilibria of system (1.2) is as follows:

(1) There is always an extinction equilibrium $E_0(0,0)$ and predator-free equilibrium $E_2(1,0)$ without any limits on parameters.
(2) When $m \in (0,1)$, which is a strong Allee effect constant, there is a predator-free equilibrium $E_1(m,0)$. Conversely, when $m \in (-1,0)$, which is a weak Allee effect constant, then $E_1(m,0)$ does not exist.
(3) The coexistence equilibrium $E_3(u_3,v_3)$ exists and it is unique when $\kappa < 2b^2(1-e)$ and $\kappa + 2b^2(e-1)m > 0$ hold, and u_3, v_3 are the positive solutions of the following equations:

$$\begin{cases} \dfrac{(1-u)(u-m)}{1+kv} - \dfrac{a(1-e)v}{\sqrt{u(1-e)+h}} = 0, \\ \dfrac{b(1-e)u}{\sqrt{u(1-e)+h}} - d = 0. \end{cases} \tag{4.3}$$

According to the second equation of (4.3), we obtain that $0 < u_3 = \frac{-\kappa}{2b^2(-1+e)} < 1$. v_3 is a positive real root less than 1 of the following quadratic equation:

$$A_2 v^2 + A_1 v + A_0 = 0,$$

where

$$A_2 = -4ab^4(-1+e)^3,$$
$$A_1 = -4akb^4(-1+e)^3,$$
$$A_0 = \left(2b^2(e-1)+\kappa\right)\sqrt{h+\frac{\kappa}{2b^2}}\left(\kappa + 2b^2(e-1)m\right),$$
$$\kappa = d(d+\sqrt{d^2+4b^2h}).$$

Since $A_2 > 0, A_1 > 0, A_0$ must be less than 0 to obtain a positive real number solution. In this case, if $A_2 + A_1 + A_0 > 0$, then otherwise there is a $v \in (0,1)$.
Overall, the coexistence equilibrium $E_3(u_3,v_3)$ exists in $S_1 = \{(a,b,d,e,h,k,m) \in R^7{}_+ | -1 < m < \frac{-\kappa}{2b^2(e-1)} \cap A_2 + A_1 + A_0 > 0\}$.

B. Stability analysis of equilibrium

In this section, we analyze the stability of the equilibrium point. First, we give the Jacobian matrix of system (1.2),

$$J = \begin{pmatrix} J_{11} & J_{12} \\ J_{21} & J_{22} \end{pmatrix},$$

where

$$J_{11} = \frac{a(e-1)(2h+u(1-e))v}{2(h+u-eu)^{\frac{3}{2}}} + \frac{(2-3u)u + m(2u-1)}{1+kv},$$
$$J_{12} = u\left(\frac{a(e-1)}{\sqrt{h+u-eu}} + \frac{k(u-1)(u-m)}{(1+kv)^2}\right),$$
$$J_{21} = -\frac{b(e-1)(2h+u-eu)v}{2(h+u-eu)^{\frac{3}{2}}},$$
$$J_{22} = -d - \frac{b(e-1)u}{\sqrt{h+u-eu}}.$$

The stability of E_0, E_1, and E_2 is shown by the following theorem.

Theorem 6:

(i) *The extinction equilibrium E_0 is locally asymptotically stable for $m \in [0,1)$ and is a saddle point for $m \in (-1,0)$;*
(ii) *the one predator-free equilibrium point $E_1(m,0)$ is locally unstable for $bm(1-e) \geq d\sqrt{h+m(1-e)}$ and is a saddle point for $bm(1-e) < d\sqrt{h+m(1-e)}$; and*
(iii) *the one prey-only equilibrium $E_2(1,0)$ is locally asymptotically stable for $b(1-e) < d\sqrt{1-e+h}$ and is a saddle point for $b(1-e) \geq d\sqrt{1-e+h}$.*

Proof. The Jacobian matrix at E_0 is calculated as follows:

$$J(E_0) = \begin{pmatrix} -m & 0 \\ 0 & -d \end{pmatrix}.$$

Obviously, the eigenvalues of $J(E_0)$ are $\lambda_1 = -m$ and $\lambda_2 = -d$, then $|\arg(\lambda_1)| = \pi > \frac{q\pi}{2}$ for $0 \leq m < 1$ or $|\arg(\lambda_1)| = 0 < \frac{q\pi}{2}$ for $-1 < m < 0$; and $|\arg(\lambda_2)| = \pi > \frac{q\pi}{2}$. By applying Theorem 3, the extinction equilibrium E_0 is locally asymptotically stable for $0 \leq m < 1$ and saddle for $-1 < m < 0$.

It is worth noting that E_1 is present when E_0 is locally asymptotically stable.

The Jacobian matrix at E_1 is

$$J(E_1) = \begin{pmatrix} m(1-m) & 0 \\ 0 & \frac{bm(1-e)-d\sqrt{h+m(1-e)}}{\sqrt{h+m-em}} \end{pmatrix}.$$

Obviously $\lambda_1 = m(1-m) > 0, \lambda_2 = \frac{bm(1-e)-d\sqrt{h+m(1-e)}}{\sqrt{h+m-em}}$ is obtained, then $|\arg(\lambda_2)| = 0 < \frac{q\pi}{2}$ for $bm(1-e) \geq d\sqrt{h+m(1-e)}$ and $|\arg(\lambda_2)| = \pi > \frac{q\pi}{2}$ for $bm(1-e) < d\sqrt{h+m(1-e)}$. By applying Theorem 3, the one predator-free equilibrium point E_1 is locally unstable for $bm(1-e) \geq d\sqrt{h+m(1-e)}$ and is a saddle point for $bm(1-e) < d\sqrt{h+m(1-e)}$.

The Jacobian matrix at E_2 is

$$J(E_2) = \begin{pmatrix} \frac{b(1-e)}{d\sqrt{1-e+h}} & 0 \\ 0 & m-1 \end{pmatrix}.$$

The eigenvalues $\lambda_1 = \frac{b(1-e)}{d\sqrt{1-e+h}}$, and $\lambda_2 = m-1 < 0$ are obtained, and $|\arg(\lambda_2)| = \pi > \frac{q\pi}{2}$. By simple calculation, $|\arg(\lambda_1)| = \pi > \frac{q\pi}{2}$ for $b(1-e) < d\sqrt{1-e+h}$ and $|\arg(\lambda_2)| = 0 < \frac{q\pi}{2}$ for $b(1-e) \geq d\sqrt{1-e+h}$. Therefore, one prey-only equilibrium E_2 is locally asymptotically stable for $b(1-e) < d\sqrt{1-e+h}$ and is a saddle point for $b(1-e) \geq d\sqrt{1-e+h}$. □

Theorem 7: *Suppose* $A_2 + A_1 + A_0 > 0$, $-1 < m < \frac{-\kappa}{2b^2(e-1)} < 0$, *and* $u_3 > m$ *hold, then the coexistence equilibrium* E_3 *is locally asymptotically stable if one of the following criteria holds:*

(i) $A_{12} + A_{13} > 0, m \in (-1, m_0)$,
(ii) $A_{12} + A_{13} > 0, m \in (m_0, 1)$ *and* $T^2 - 4D < 0, 0 < q < q^*$,
(iii) $A_{12} + A_{13} < 0, m \in (0, m_0)$, *and*
(iv) $A_{12} + A_{13} < 0, m \in (m_0, 1)$ *and* $T^2 - 4D < 0, 0 < q < q^*$,

where

$$m_0 = -\frac{\sqrt{2}a(e-1)^2 v(kv+1)}{(\kappa + 2hb^2)^{\frac{3}{2}}} - \frac{\kappa}{b^2(e-1)} - 1.$$

Proof. Assuming $u_3 > m$, we can obtain the Jacobian matrix of system (1.2) at E_3 as follows:

$$J(E_3) = \begin{pmatrix} J_{11}(E_3) & J_{12}(E_3) \\ J_{21}(E_3) & J_{22}(E_3) \end{pmatrix}, \tag{4.4}$$

where

$$J_{11}(E_3) = \frac{a(e-1)^2 u_3 v_3}{2(h + u_3 - eu_3)^{\frac{3}{2}}} + \frac{(1 + m - 2u_3)u_3}{1 + kv_3},$$

$$J_{12}(E_3) = u_3 \left(\frac{a(e-1)}{\sqrt{h + u_3 - eu_3}} + \frac{k(u_3 - 1)(u_3 - m)}{(1 + kv_3)^2} \right),$$

$$J_{21}(E_3) = -\frac{b(e-1)(2h + u_3 - eu_3)v_3}{2(h + u_3 - eu_3)^{\frac{3}{2}}},$$

$$J_{22}(E_3) = 0.$$

The corresponding characteristic equation for $J(E_3)$ is $\lambda^2 - T\lambda + D = 0$, and the two eigenvalues satisfy $\lambda_1\lambda_2 = -J_{12}J_{21} > 0, \lambda_1 + \lambda_2 = T$,

$$T = Tr(J(E_3)) = J_{11}(E_3) + J_{22}(E_3) = \frac{a(e-1)^2 u_3 v_3}{2(h + u_3 - eu_3)^{\frac{3}{2}}} + \frac{(1 + m - 2u_3)u_3}{1 + kv_3},$$

$$D = Tr(J(E_3)) = J_{11}(E_3)J_{22}(E_3) - J_{12}(E_3)J_{21}(E_3) = p_2 v_3^3 + 2kp_2 v_3 + p_1,$$

$$p_2 = \frac{ab(e-1)^2 k^2 u(2h + u - eu)}{2(kv+1)^2(-eu + h + u)^2},$$

$$p_1 = \frac{b(e-1)u((e-1)u - 2h)\left(hk(u-1)(m-u) - (e-1)\left(a\sqrt{-eu + h + u} + k(u-1)u(m-u)\right)\right)}{2(kv+1)^2(h + u - eu)^{5/2}}.$$

Applying Theorem 3, if $T < 0$, then λ_1 and λ_2 are non-negative real roots, i.e., $|\arg(\lambda_{1,2})| = \pi > \frac{q\pi}{2}$; if $T = 0$, then the two eigenvalues are pure imaginary roots that meet $|\arg(\lambda_{1,2})| = \frac{\pi}{2} > \frac{q\pi}{2}$. In this case, E_3 is locally asymptotically stable. If $T > 0$ and $T^2 - 4D < 0$ hold, then the two eigenvalues are a pair of complex conjugate roots with positive real parts: $\lambda_{1,2} = \frac{T}{2} \pm \frac{\sqrt{4D - T^2}i}{2}$, by calculating $|\arg(\lambda_{1,2})| = \tan^{-1}\frac{\sqrt{4D-T^2}}{T}$ to obtain $q = q^*$. In this case, if $\tan^{-1}\frac{\sqrt{4D-T^2}}{T} > \frac{q\pi}{2}$, i.e., $0 < q < q^*$ holds, E_3 is locally asymptotically stable. Since $a(e-1)^2 v(kv+1) + 2(m - 2u + 1)(u + h + u - e)^{3/2} > 0$ determines the positive and negative aspects of T, we combine like terms with the Allee effect m as the variable to obtain

$$f_1 = A_{11}m + A_{12} + A_{13},$$

where $A_{11} = \frac{(\kappa + 2hb^2)^{\frac{3}{2}}}{\sqrt{2}} > 0$, $A_{12} = \frac{(\frac{\kappa}{b^2} + 2h)^{\frac{3}{2}}(\kappa + b^2(e-1))}{\sqrt{2}b^2(e-1)} < 0, A_{13} = a(e-1)^2 v(kv+1) > 0$. Thus, the zero m_0 of f_1 is influenced by $A_{12} + A_{13}$ positive and negative.

When $A_{12} + A_{13} > 0$, $m_0 < 0$ and $f_2 = m_0 + 1 = B_{11}v^2 + B_{12}v + B_{13}$, where $B_{11} = -\frac{\sqrt{2}a(e-1)^2 k}{(\kappa + 2hb^2)^{\frac{3}{2}}} < 0, B_{12} = -\frac{\sqrt{2}a(e-1)^2}{(\kappa + 2hb^2)^{\frac{3}{2}}} < 0$, $B_{13} = -\frac{\kappa}{b^2(e-1)} > 0$. Since $v \in (0,1)$, the axis of symmetry of f_2 is negative, so $m_0 \in (-1, 0)$. When $A_{12} + A_{13} < 0$, $m_0 > 0$ and $f_3 = m_0 - 1 = B_{11}v^2 + B_{12}v + C_0$, so for $B_{11} + B_{12} + B_{13} > 0$, $m_0 \in (0,1)$ where $C_0 = -\frac{\kappa}{b^2(e-1)} - 2 < 0$.

Overall, E_3 is locally asymptotically stable when (i), (ii), (iii), and (iv) are satisfied. □

Theorem 8: *The coexistence equilibrium* $E_3(u_3, v_3)$ *is globally asymptotically stable if* $\eta_1 < 0$, $\eta_2 < 0$, *and* $\eta_3 < 0$ *hold, where* $\eta_1 = \eta - m$, $\eta_2 = \frac{a(1-e)\eta}{\sqrt{(1-e)\eta + h}}$, $\eta_3 = u_3(1-\eta)(\eta - m)$.

TABLE II. Equilibrium point stability type for system (1.2).

E_0	E_1	E_2	E_3
$m \in (-1, 0)$, Saddle points	No existence	LAS	No existence (see Fig. 1), $\kappa \geq 2b^2(e-1)$
		Saddle points	Nodes (see Fig. 2), $A_{12}+A_{13}>0, m \in (-1, m_0)$ or $A_{12}+A_{13}<0$
			Stable focus (see Fig. 3), $A_{12}+A_{13}>0, m \in (m_0, 0), T^2-4D<0, 0<q<q^*$
			Unstable focus (see Fig. 4), $A_{12}+A_{13}>0, m \in (m_0, 0), T^2-4D<0, q^*<q<1$
$m \in (0, 1)$, LAS	Saddle points	Saddle points	Nodes (see Fig. 5), $A_{12}+A_{13}<0, m \in (0, m_0)$
			Stable focus (see Fig. 6), $A_{12}+A_{13}>0, T^2-4D<0, \tan^{-1} 0<q<q^*$
			Source (see Fig. 7), $T^2-4D>0, A_{12}+A_{13}<0, m \in (m_0, 1)$ or $A_{12}+A_{13}>0$
			Unstable focus (see Fig. 8), $A_{12}+A_{13}<0, m \in (m_0, 1), T^2-4D<0, q^*<q<1$, or $A_{12}+A_{13}>0, T^2-4D<0, q^*<q<1$
		LAS	No existence (see Fig. 9), $\kappa \geq 2b^2(e-1)$

Proof. Construct the function as follows:

$$V(t) = V(u, v) = \left(u - u_3 - u_3 \ln \frac{u}{u_3}\right) + \frac{a}{b}\left(v - v_3 - v_3 \ln \frac{v}{v_3}\right).$$

By calculating the q order derivative of $V(u, v)$ along with the solution, we have

$$\begin{aligned}
{}_0^C D_t^q V(t) &\leq \frac{u-u_3}{u} \cdot {}^C D_t^q u + \frac{a(v-v_3)}{bv} \cdot {}^C D_t^q v \\
&= (u-u_3)\left(\frac{(1-u)(u-m)}{1+kv} - \frac{a(1-e)v}{\sqrt{u(1-e)+h}}\right) \\
&\quad + (v-v_3)\left(\frac{a(1-e)u}{\sqrt{u(1-e)+h}} - d\right) \\
&\leq u(\eta - m) + \frac{a(1-e)\eta v}{\sqrt{(1-e)\eta + h}} \\
&\quad + u_3(1-\eta)(\eta - m) \\
&\doteq u\eta_1 + v\eta_2 + \eta_3,
\end{aligned}$$

where $\max\{|u|, |v|\} \leq \eta$. If $\eta_1 < 0$, $\eta_2 < 0$, and $\eta_3 < 0$ hold, then ${}_0^C D_t^q V(t) \leq 0$, i.e., $V(t)$ is a Lyapunov function. Therefore, the coexistence equilibrium $E_3(u_3, v_3)$ is globally asymptotically stable. □

We provide the existence and stability of all equilibrium points of system (1.2), as shown in Table II (locally asymptotically stable for LAS for brevity).

Remark 1: *The current section aims to investigate the stability properties of the equilibrium points of system (1.2), which can be categorized as the strong Allee effect, the weak Allee effect, and no Allee effect, based on the value of parameter m. Specifically, when $m \in (0, 1)$, system (1.2) exhibits a strong Allee effect, resulting in the local asymptotic stability of E_0 and the saddle point or local instability of E_1. Conversely, when $m = 0$, no Allee effect is observed, causing E_0 and E_1 to collide and coincide at E_0 while maintaining the stability of E_0. With the weak Allee effect, with $m \in (-1, 0)$, E_1 disappears, and E_0 becomes a saddle point. Furthermore, the presence of E_3 affects the stability of E_2, where E_2 is a saddle point if E_3 exists but locally asymptotically stable if E_3 does not exist. Table II summarizes the relationships between the equilibrium points and their corresponding stability properties. It is worth noting that in Figs. 2 and 3, the appearance of E_3 leads to its global asymptotic stability.*

Remark 2: *According to the theorems presented in this study, the dynamics of a predator–prey system are influenced by the strength of the Allee effect exhibited by the prey population. In the case of weak Allee effects, the system can exhibit three distinct scenarios regardless of the initial densities of both populations. If both populations converge toward E_2, the predator population faces extinction, as depicted in Fig. 1. Conversely, if the coexisting equilibrium point E_3 is globally asymptotically stable, as illustrated in Figs. 2 and 3, the populations tend to coexist. Finally, when a stable limit cycle near E_3 exists, as shown in Fig. 4, all initial density orbits converge toward this limit cycle.*

However, in the case of strong Allee effects exhibited by the prey population, a low initial density of the prey population leads to its attraction toward the basin of attraction of E_0. This ultimately results in the extinction of the predators and the prey population, with the emergence of the extinction equilibrium point E_1. The stable manifold of E_1 acts as a dividing line, separating the first quadrant into two distinct regions, the attraction zone of E_0, and the stable path of E_2 (see Figs. 5–9). In the presence of a coexisting equilibrium E_3, three main situations arise. If the coexistence equilibrium E_3 is locally stable, predators in the second region are subject to the Allee effect, causing them to move toward coexistence when they are about to become extinct (see Figs. 5 and 6). Regardless of the initial sizes of the two populations, the system eventually leads to the extinction of both populations (see Fig. 7). Alternatively, the two populations may be attracted to a stable limit cycle near the coexisting equilibrium E_3 (see Fig. 8). Conversely, when coexistence equilibrium E_3 does not exist, the isotropic line of E_1 splits the first quadrant into two regions, where either the two populations become extinct or the predator perishes and the prey flourishes (see Fig. 9). The above findings have

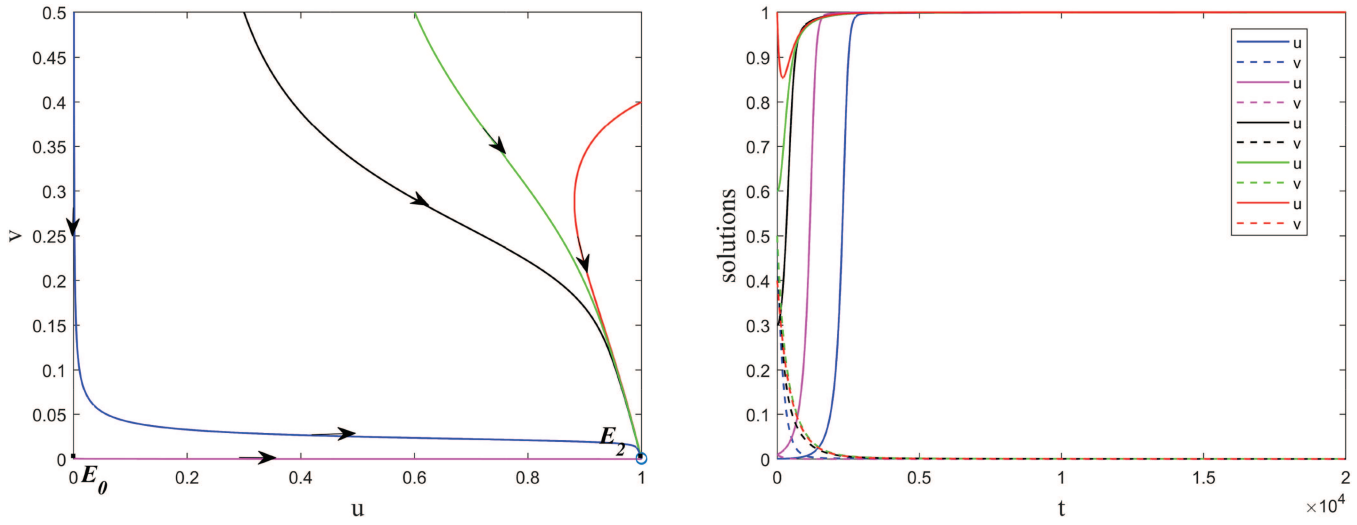

(a) (b)

FIG. 1. (a) and (b) are the phase diagram and solution curves of system (1.2) with initial values (0.001, 0.5) in blue, (0.001, 0.001) in rose red, (0.4, 0.5) in black, (0.6, 0.5) in green, and (1, 0.4) in red, respectively.

significant implications for ecological conservation efforts, particularly in populations exhibiting the Allee effect.

C. Bifurcation analysis

We choose the prey with Allee effect m, the death rate of the prey population b, the death rate of the predator population d, prey protection effect e, threshold for the transition between herd grouping and solitary behavior h, and the fractional order q as bifurcation parameters to investigate the bifurcation of system (1.2) at the coexistence equilibrium.

Theorem 9: *Assuming $J_{11} > 0$ and $T^2 - 4D < 0$, system (1.2) experiences a Hopf bifurcation near E_3 at $m = m^*$ and a stable limit cycle around E_3, where*

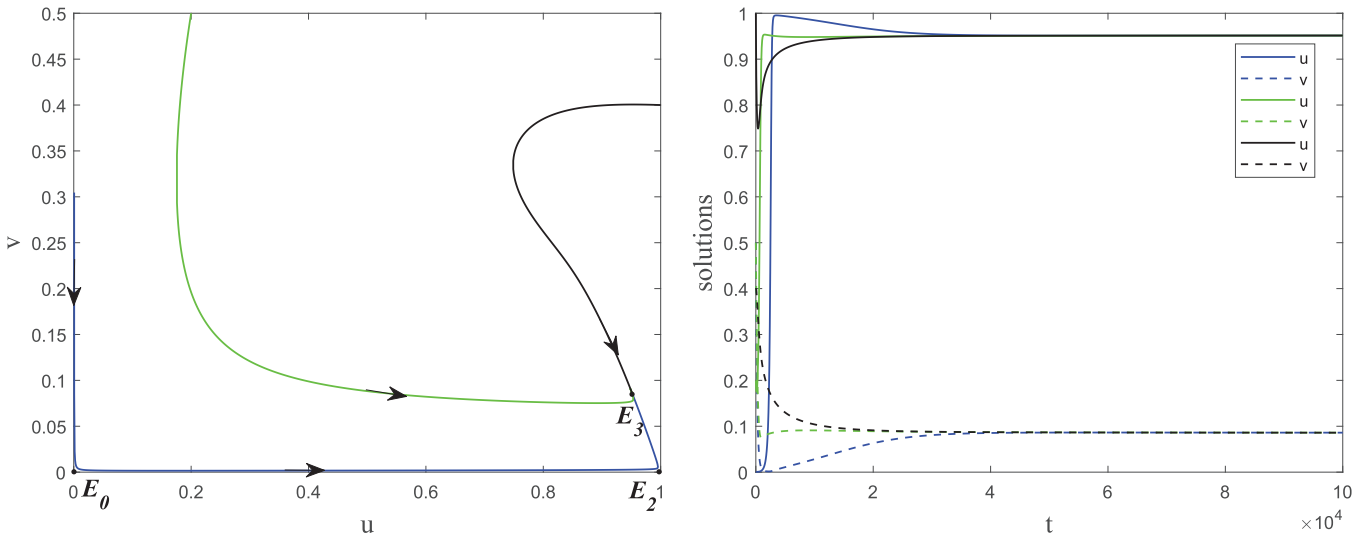

(a) (b)

FIG. 2. (a) and (b) are the phase diagram and solution curves of system (1.2) with initial values (0.001, 0.3) in blue, (0.2, 0.5) in green, and (1, 0.4) in black, respectively.

$$\left(\frac{\sqrt{4D-T^2}}{T}\right)\Big|_{m=m^*} = \tan\frac{q\pi}{2} \text{ and } \frac{d}{dm}\left(\frac{\sqrt{4D-T^2}}{T}\right)\Big|_{m=m^*} \neq 0.$$

Proof. When $J_{11} > 0$ and $4D - T^2 > 0$ meet, the Jacobian matrix $J(E_3)$ has a couple of conjugate complex solutions $\lambda_{1,2} = \frac{T}{2} \pm \frac{\sqrt{4D-T^2}}{2}i$, and $|\arg(\lambda_{1,2})| = \tan^{-1}\frac{\sqrt{4D-T^2}}{T}$. If $\left(\frac{\sqrt{4D-T^2}}{T}\right)\Big|_{m=m^*} = \tan\frac{q\pi}{2}$ meets, then $|\arg(\lambda_{1,2})|_{m=m^*} = \frac{q\pi}{2}$. If $\frac{d}{dm}\left(\frac{\sqrt{4D-T^2}}{T}\right)\Big|_{m=m^*} \neq 0$ meets, then

$$\frac{d}{dm}|\arg(\lambda_{1,2})|_{m=m^*} = \frac{T^2}{T^2-4D}\frac{d}{dm}\left(\frac{\sqrt{4D-T^2}}{T}\right)\Big|_{m=m^*} \neq 0.$$

The singularity condition requires that the real part of the eigenvalues associated with the Hopf bifurcation be greater than zero. The section condition requires that the derivative of the mode of the eigenvalues with respect to the bifurcation parameter is nonzero. Together, these conditions ensure that a stable limit cycle emerges around E_3 as parameter m varies.

Overall, in addition to the conditions for the Hopf bifurcation, if the singularity and cross-section conditions of the Hopf bifurcation are also satisfied, then model (1.2) experiences a Hopf bifurcation around E_3 at $m = m^*$.

Note that we can use the same method to analyze the bifurcation of the system at b, d, e, h, respectively. □

Theorem 10: *Suppose $J_{11} > 0$ and $T^2 - 4D < 0$, then system (1.2) experiences a Hopf bifurcation around E_3 at $q = q^*$, where $q^* = \frac{2}{\pi}\tan^{-1}\left(\frac{\sqrt{4D-T^2}}{T}\right)$.*

Proof. Under the conditions $J_{11} > 0$ and $T^2 - 4D < 0$, the Jacobian matrix $J(E_3)$ has a pair of conjugate complex eigenvalues $\lambda_{1,2} = \frac{T}{2} \pm \frac{\sqrt{4D-T^2}}{2}i$. To check if the conditions for Hopf bifurcation are met, we define

$$\psi_{1,2}(q) = \frac{q\pi}{2} - |\arg(\lambda_{1,2})|$$

and evaluate them at $q = q^*$, where q^* is given by $\tan\frac{q^*\pi}{2} = \frac{\sqrt{4D-T^2}}{T}$.

If $\psi_{1,2}(q^*) = 0$ and $\frac{d\psi_{1,2}}{dq}(q^*) \neq 0$, then the conditions for Hopf bifurcation are satisfied, and system (1.2) experiences a Hopf bifurcation around E_3 at $q = q^*$. □

Remark 3: *The equilibrium analysis presented in Table II demonstrates the clear influence of the strength of the Allee effect on the existence and stability of equilibrium points. In the case of weak Allee effects, E_0 and E_2, are found to be saddle points, while E_3 is unstable, leading to the emergence of a limit cycle around it. All system solutions are observed to approach this limit cycle from their initial points. Without the Allee effect, E_0 is locally stable, while E_2 and E_3 remain unaffected, and the limit cycle expands considerably. On the other hand, for strong Allee effects, the stability of E_0, E_2, and E_3 remains unchanged, and a new saddle point, E_1, appears. As a result, the soliton starting from (1, 0.6) enters E_1 and reaches E_0 instead of being attracted to the limit cycle. However, the solution trajectory originating from the right neighborhood of E_1 approaches the limit cycle through E_2 (see Fig. 10).*

Remark 4: *System (1.2) exhibits a Hopf bifurcation around equilibrium point E_3, depending on the strength of the Allee effect, as parameterized by b. The system exhibits distinct Hopf bifurcations for different levels of the Allee effect, as illustrated in Figs. 11 and 12. For weak Allee effects, the system's behavior is akin to the m bifurcation*

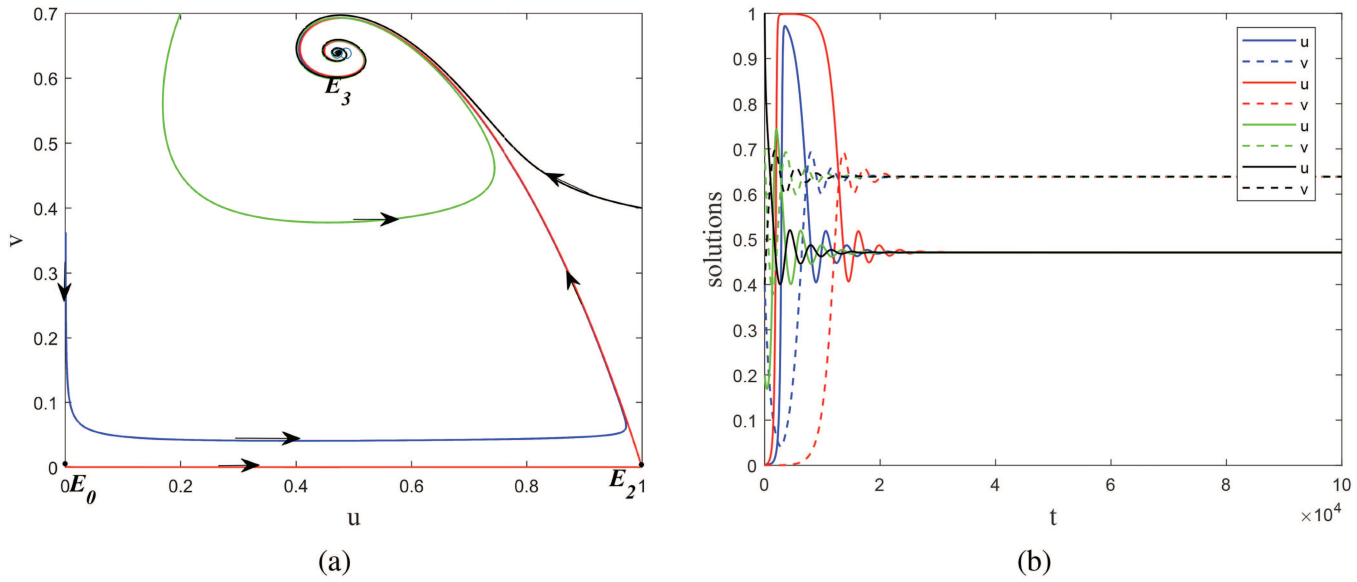

FIG. 3. (a) and (b) are the phase diagram and solution curves of system (1.2) with initial values (0.001, 0.36) in blue, (0.001, 0.001) in rose red, (0.2, 0.7) in green, and (1, 0.4) in black, respectively.

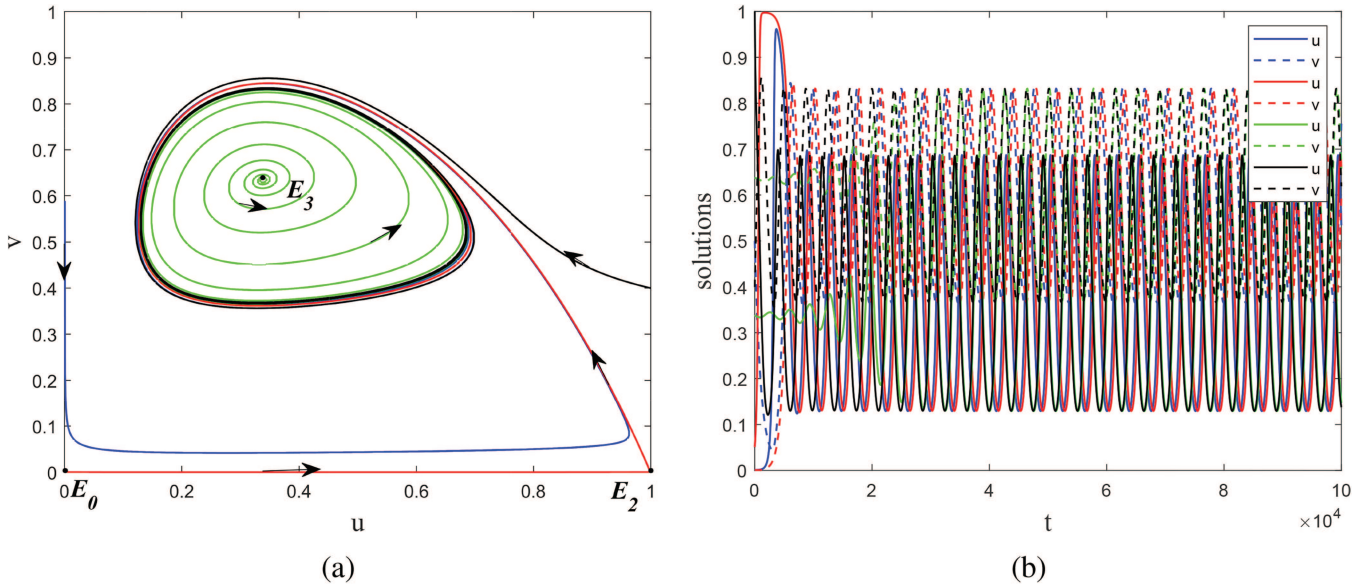

FIG. 4. (a) and (b) are the phase diagram and solution curves of system (1.2) with initial values (0.001, 0.6) in blue, (0.001, 0.001) in rose red, (0.338, 0.637) in green, and (1, 0.4) in black, respectively.

parameter [see Figs. 11(a) and 11(b)]. In contrast, under strong Allee effects, the equilibrium point E_3 becomes an unstable focus, and a stable limit cycle forms around it, while E_0 becomes locally stable, and E_1 and E_2 transform into saddle points (see Fig. 12). As b increases, the system trajectory evolves from being attracted to the limit cycle to redirecting toward E_1 and eventually reaching E_0 from the initial point (1,0.6). This process results in an increase in the limit cycle's size. Moreover, the solution orbit from the right neighbor of E_1 approaches the limit cycle via E_2. It is worth noting that a similar trend is observed for the parameters d, e, and h.

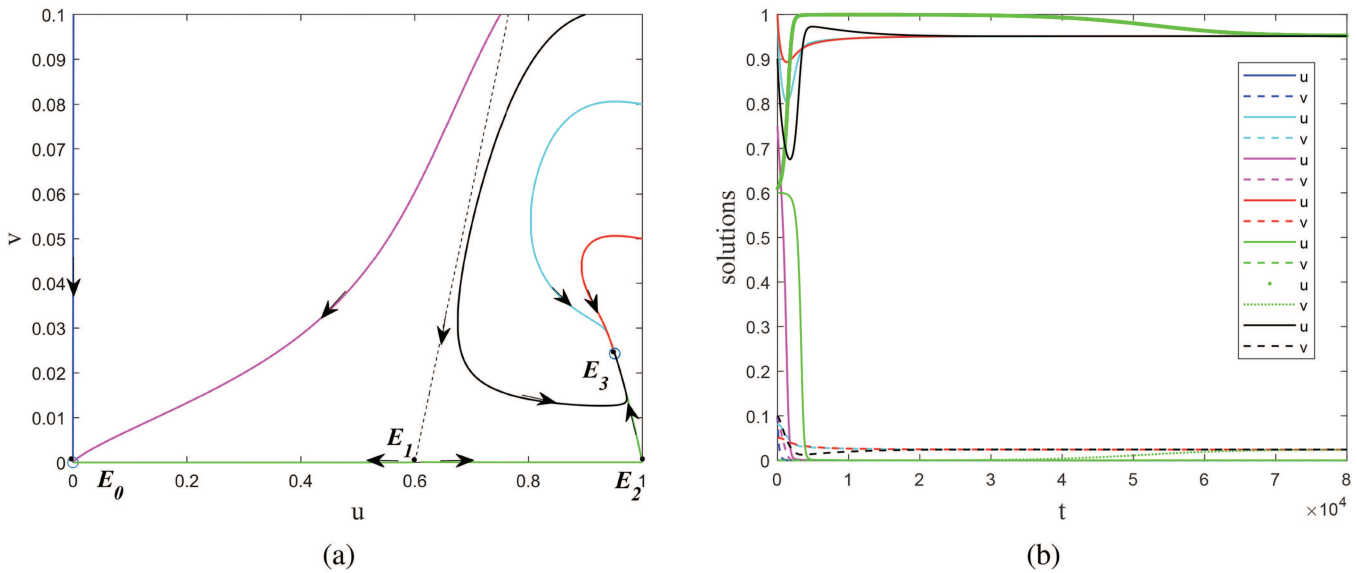

FIG. 5. (a) and (b) are the phase diagram and solution curves of system (1.2) with initial values (0.001, 0.6) in blue, (0.6, 0.001) in lime green, (0.601, 0.001) in green, (0.75, 0.1) in rose red, (0.9, 0.1) in black, (1, 0.08) in lime green, (1, 0.05) in red, and (0.76, 0.1) in dashed line, respectively.

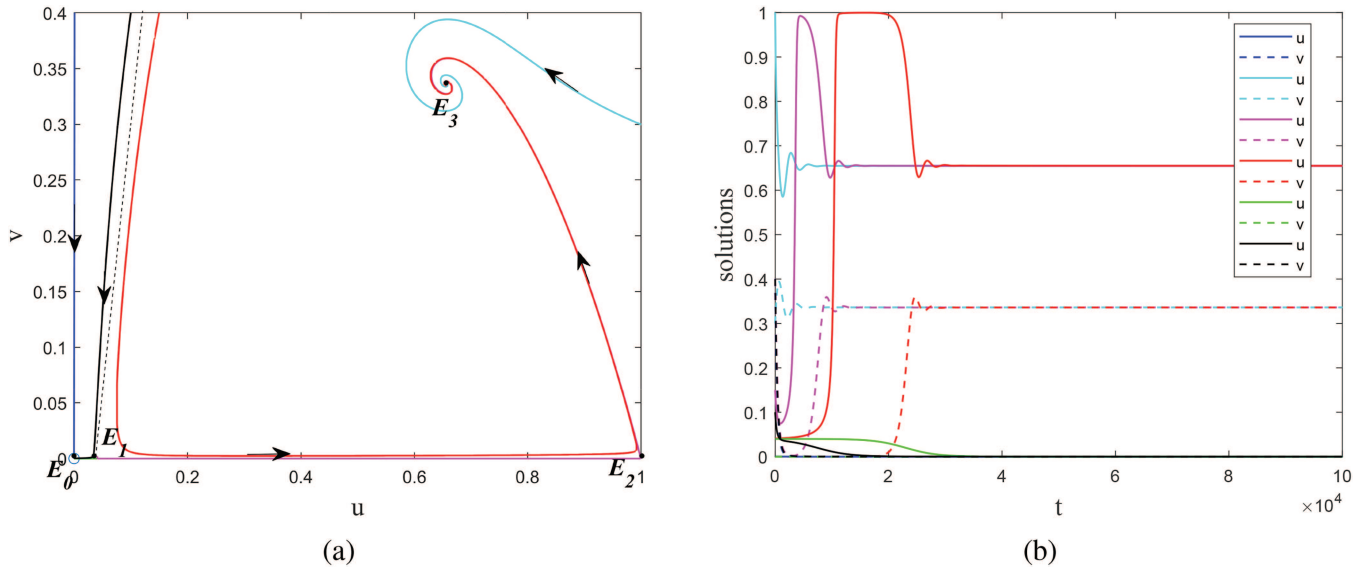

FIG. 6. (a) and (b) are the phase diagram and solution curves of system (1.2) with initial values (0.001, 0.6) in blue, (0.1, 0.4) in black, (0.15, 0.4) in red, (0.04, 0.001) in green, (0.041, 0.001) in rose red, (1, 0.3) in lime green, and (0.17, 0.4) in dashed line, respectively.

Remark 5: *The equilibrium point E_3 in system (1.2) undergoes a Hopf bifurcation, which is determined by parameter q, as shown in Figs. 22 and 23. The impact of Allee effects on the bifurcation and phase diagrams is evident. Notably, the emergence of a limit cycle is associated with the bifurcation at $q \to 1$, and its size increases as $q \to 1$. Conversely, the system stabilizes as $q \to 0$. Clearly, when $q = 1$, it can be analyzed using the classical theory of Hopf bifurcation in integer-order differential equations. Consequently, it is possible to eliminate the limit cycle by reducing the order of the fractional-order system, thereby increasing its stability. If the initial densities of the*

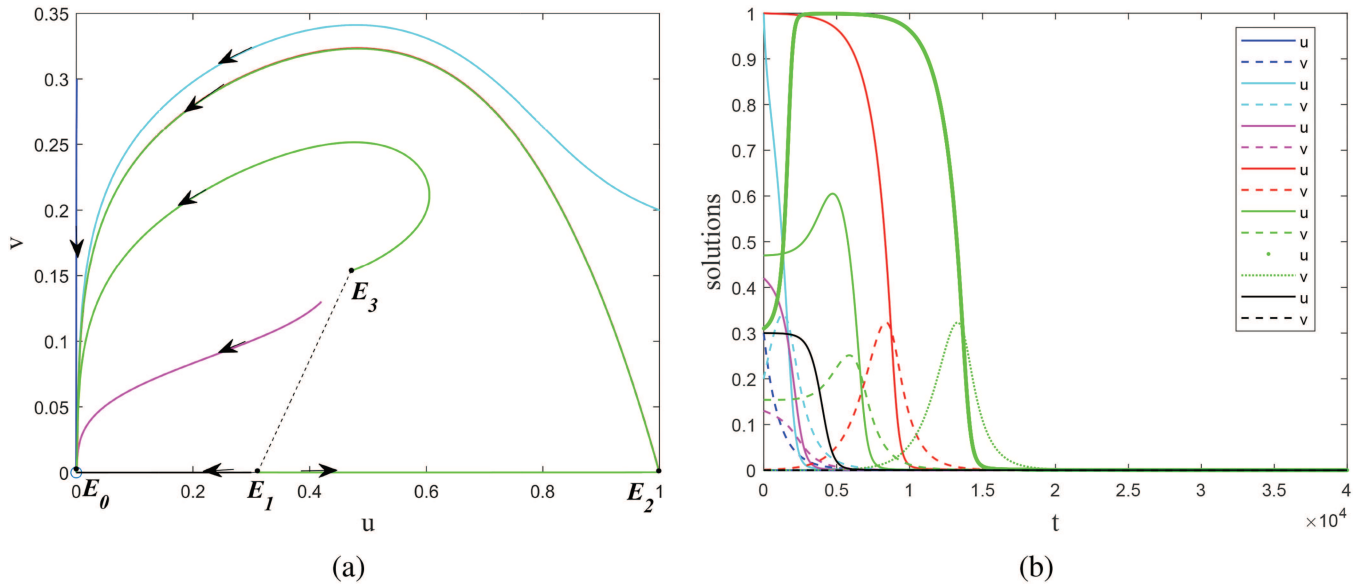

FIG. 7. (a) and (b) are the phase diagram and solution curves of system (1.2) with initial values (0.001, 0.6) in blue, (0.3, 0.001) in black, (0.301, 0.001) in green, (0.42, 0.13) in rose red, (0.47, 0.153) in green, (1,0.2) in lime green, and (0.47, 0.153) in dashed line, respectively.

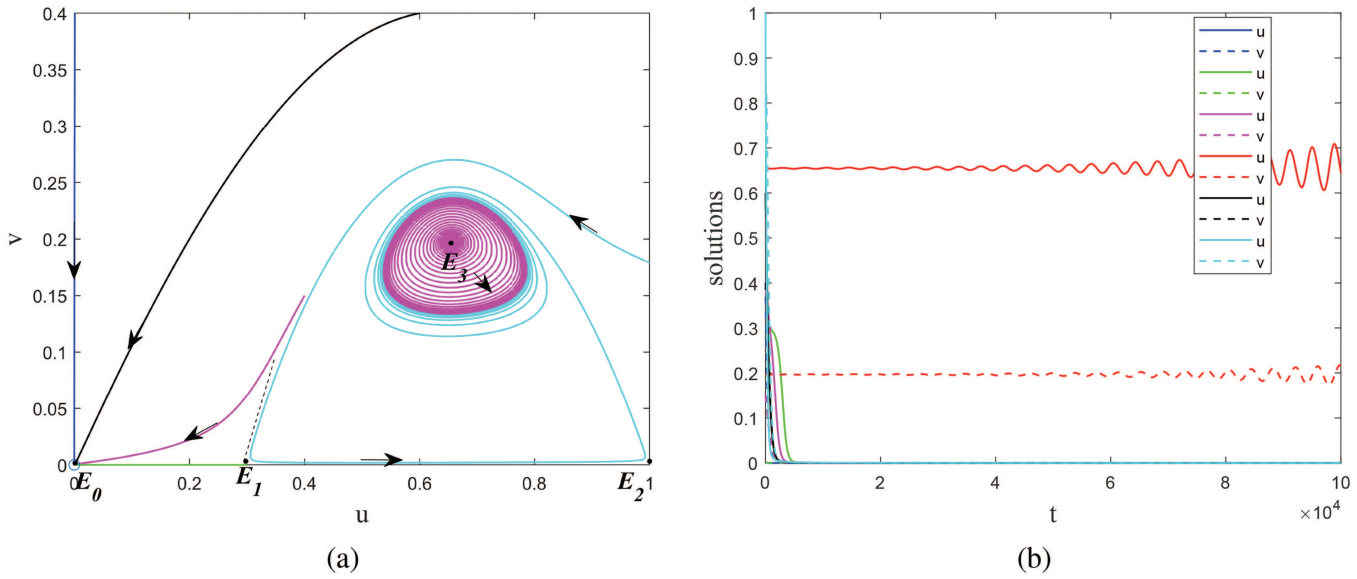

FIG. 8. (a) and (b) are the phase diagram and solution curves of system (1.2) with initial values (0.001, 0.6) in blue, (0.3, 0.001) in green, (0.4, 0.15) in rose red, (0.6, 0.4) in black, (0.655, 0.197) in red, (1, 0.1791) in lime green, and (0.3, 0.09) in dashed line, respectively.

two species in system (1.2) do not fall within the attraction domain of the extinction equilibrium point and the system has a coexistence equilibrium, the limit cycle can be eliminated. This finding highlights the superior stability of the fractional-order system compared to the integer-order system.

V. SYSTEM (1.2) DISCRETE ANALYSIS

To discretize system (1.2), we will employ the method described in Ref. 57. Specifically, we will utilize a piecewise constant argument in our discretization. The expression gives the resulting

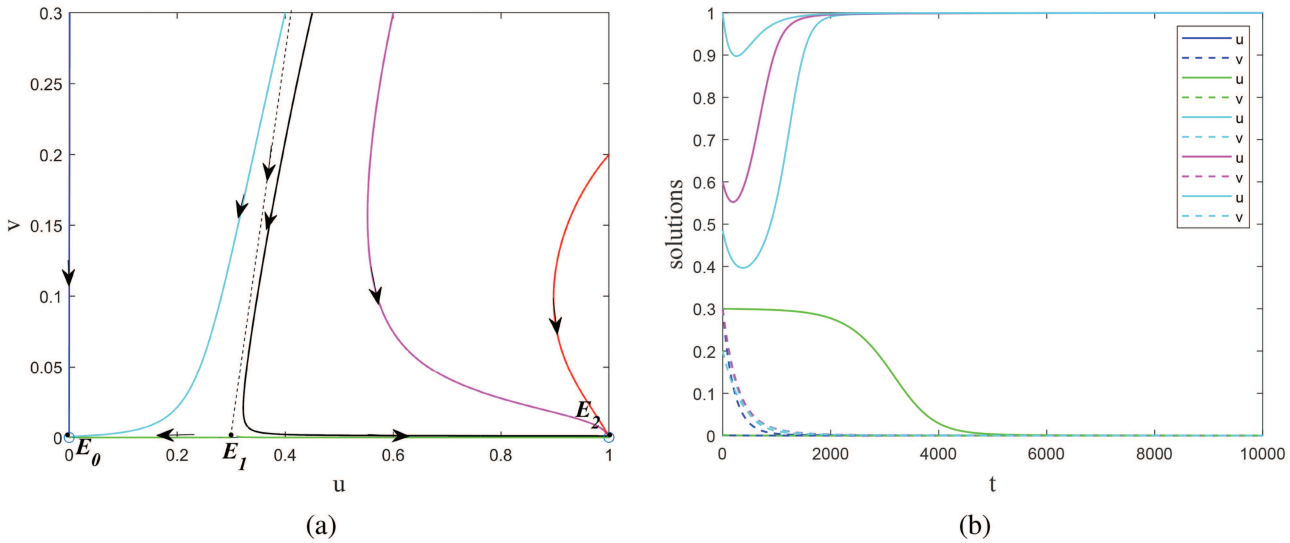

FIG. 9. (a) and (b) are the phase diagram and solution curves of system (1.2) with initial values (0.001, 0.6) in blue, (0.3, 0.001) in green, (0.301, 0.001) in lime green, (0.42, 0.3) in black, (0.485, 0.3) in lime green, (0.6, 0.3) in rose red, (1, 0.2) in rose red, and (0.4, 0.3) in dashed line, respectively.

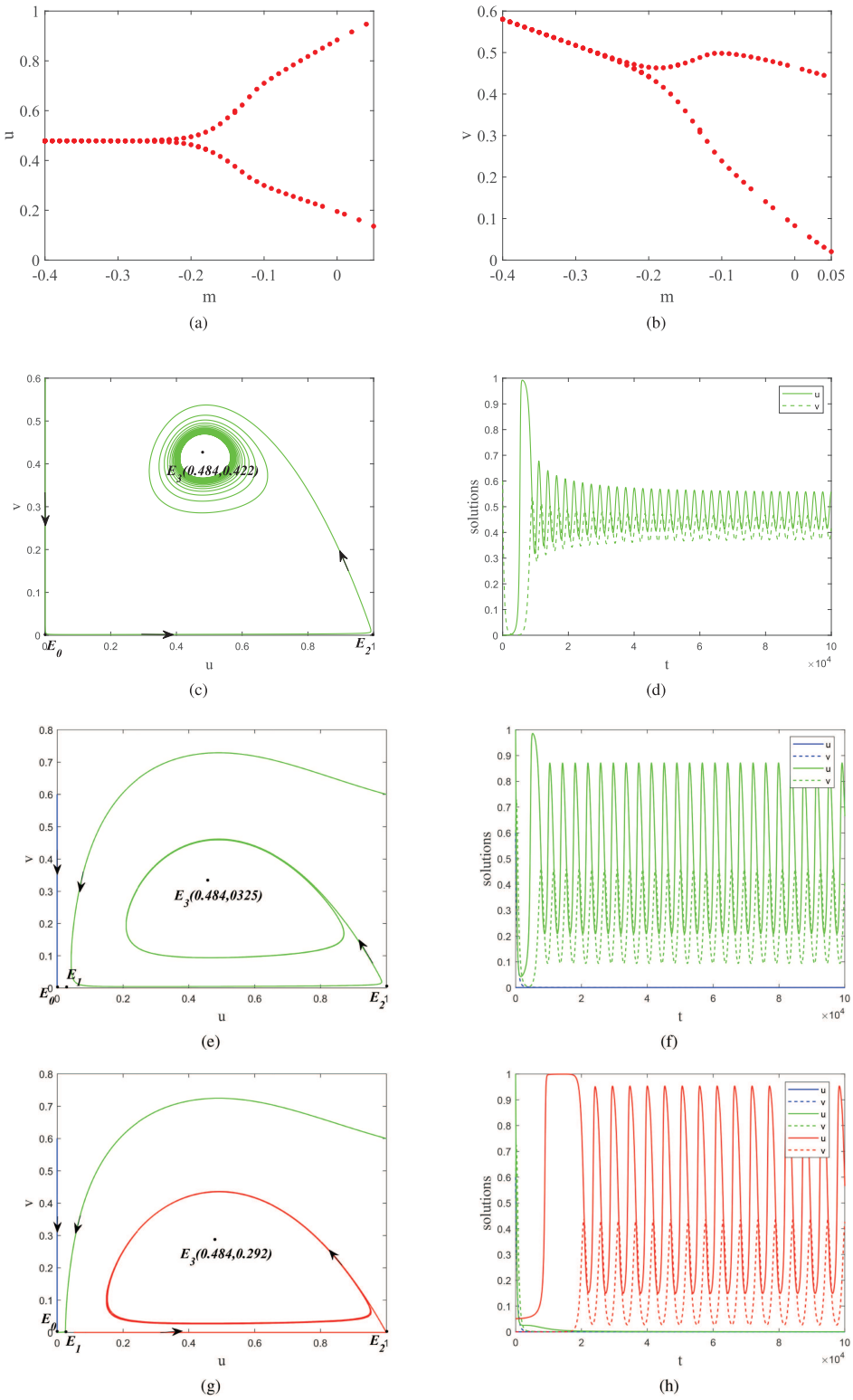

FIG. 10. (a) and (b) are bifurcation diagrams with parameter m for $q = 0.98$; (c) and (d) are the phase diagram and solution curves of system (1.2) with initial value $(0.001, 0.6)$ in green and $m = -0.15$, respectively. (e) and (f) are the phase diagram and solution curves of system (1.2) with initial values $(0.001, 0.6)$ in blue, and $(1, 0.6)$ in green and $m = 0$, respectively; (g) and (h) are the phase diagram and solution curves of system (1.2) with initial values $(0.001, 0.6)$ in blue, $(0.051, 0.001)$ in red, and $(1, 0.6)$ in green and $m = 0.05$, respectively.

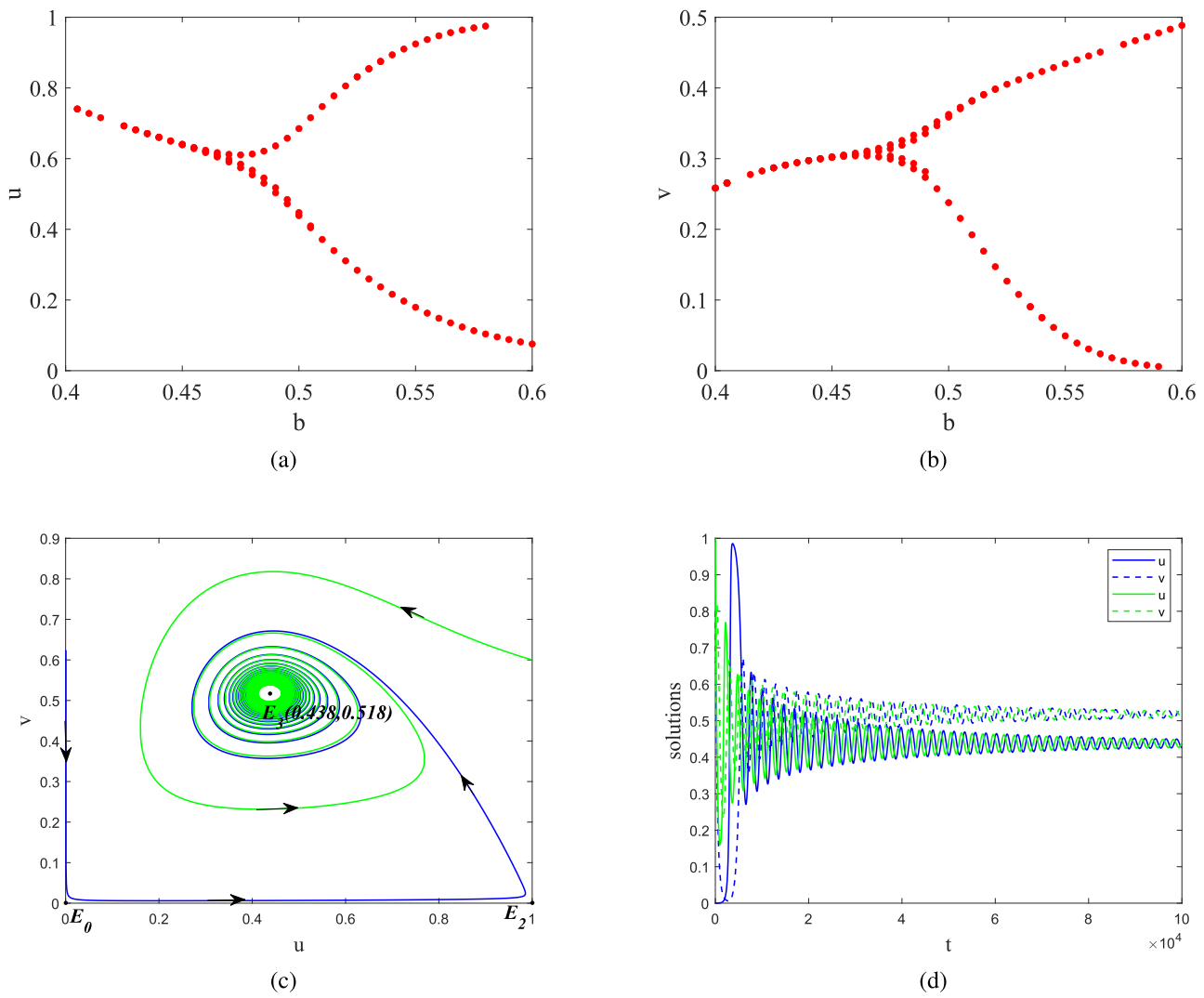

FIG. 11. (a) and (b) are bifurcation diagrams with parameter b for $m = -0.3$, $q = 0.98$; (c) and (d) are the phase diagram and solution curves of system (1.2) with initial value $(0.001, 0.6)$ in blue, and $(1, 0.6)$ in green and $b = 0.6$, $m = -0.3$, respectively.

discretized system,

$$u_{n+1} = u_n + \frac{\varsigma^q}{\Gamma(1+q)}\left(-\frac{a(1-e)u_n v_n}{\sqrt{h+(1-e)u}} + \frac{(1-u_n)u_n(-m+u_n)}{1+kv_n}\right),$$
$$v_{n+1} = v_n + \frac{\varsigma^q}{\Gamma(1+q)}\left(-dv_n + \frac{b(1-e)u_n v_n}{\sqrt{h+(1-e)u_n}}\right), \tag{5.5}$$

which represents a numerical approximation of the original system (1.2). It is worth noting that discretization is a widely used technique to approximate the dynamics of continuous systems. In the case of non-integer order systems such as (1.2), piecewise constant approximation is an effective method for approximating non-integer order derivatives. The resulting discrete system can be solved numerically through a variety of methods, such as finite difference or Runge–Kutta techniques, to yield numerical solutions. Thus, discretization is a crucial step in the analysis of the behavior of the system.

Despite the approximation process, which involves converting continuous systems into discrete ones, the equilibrium point of the system remains unchanged. This study focuses on two primary investigations related to the discretized system. First, we examine the effect of the step size, a critical parameter in the discretization process, on the stability of the system. Second, we explore the potential emergence of increased complexity in the dynamic

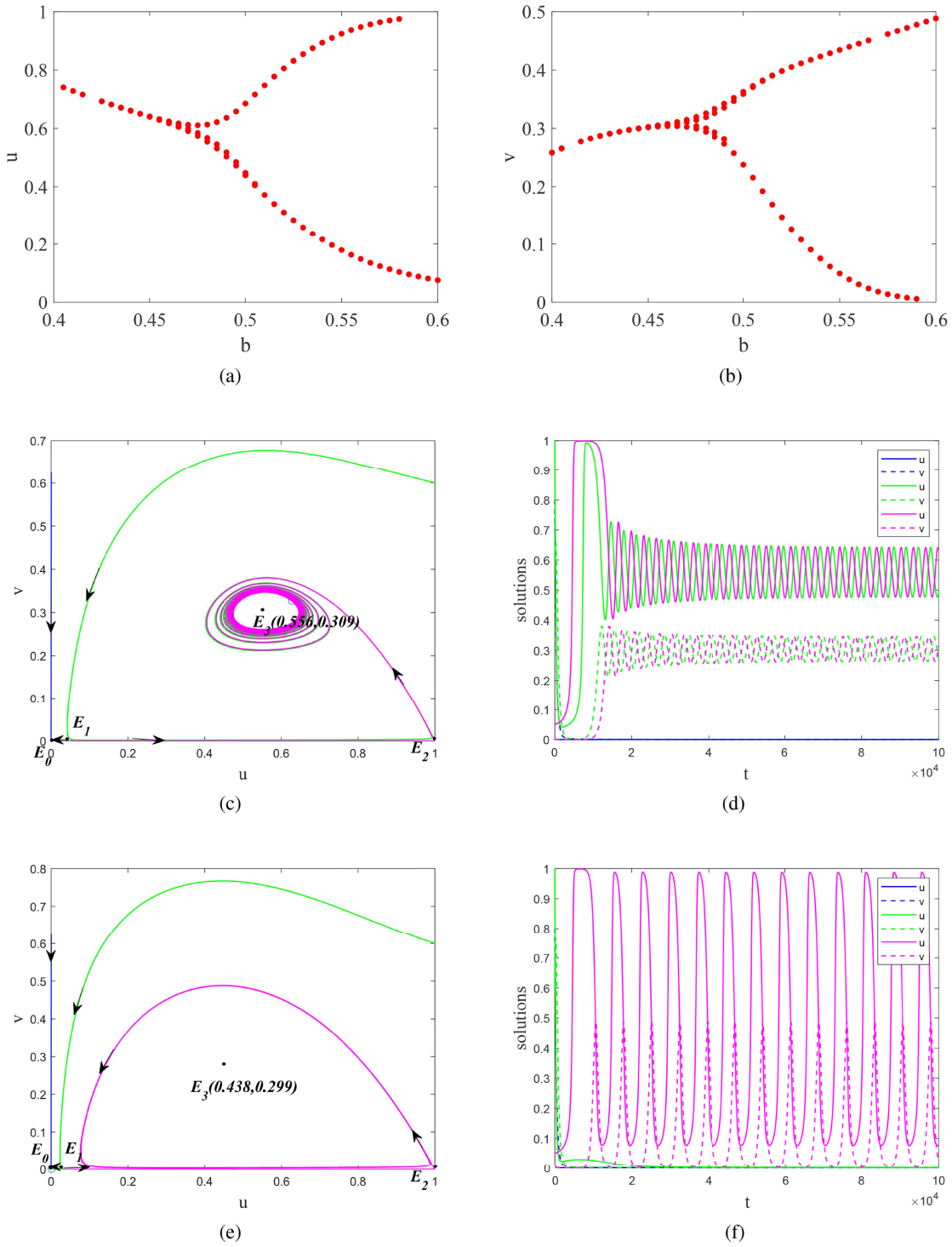

FIG. 12. (a) and (b) are bifurcation diagrams with parameter b for $m = 0.04, q = 0.98$; (c) and (d) are the phase diagram and solution curves of system (1.2) with initial values (0.001, 0.6) in blue, (1, 0.6) in green, (0.041,0.001) in rose red and $b = 0.5, m = 0.04$, respectively; (e) and (h) are the phase diagram and solution curves of system (1.2) with initial values (0.001, 0.6) in blue, (1, 0.6) in green, and (0.041, 0.001) in rose red and $b = 0.6, m = 0.04$, respectively.

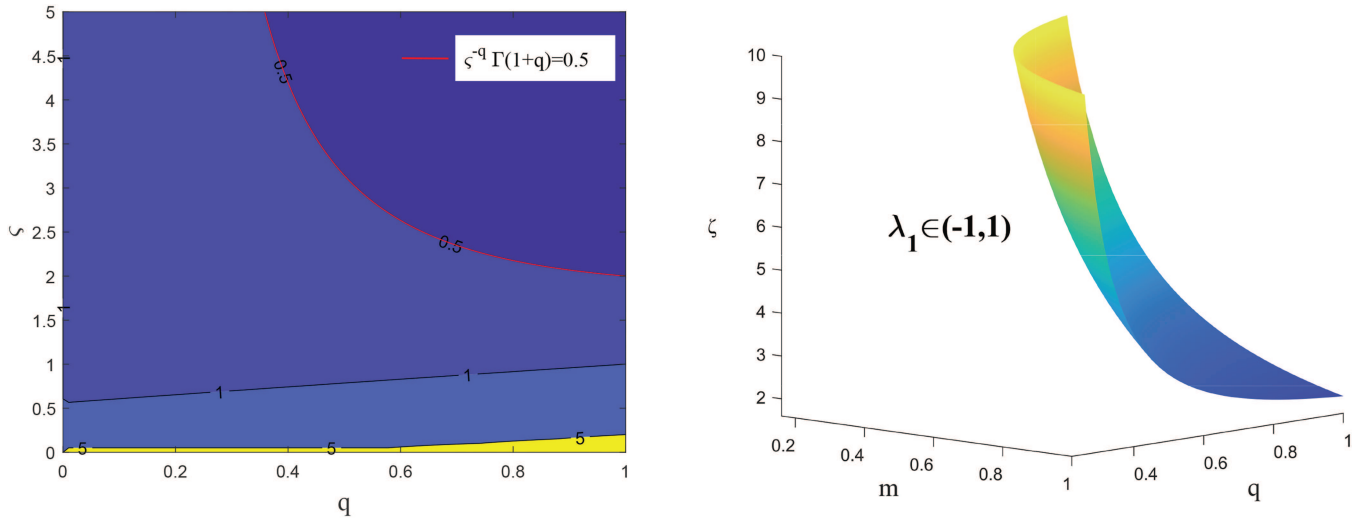

FIG. 13. (a) is a graph of the densities of ς and q; (b) is the surface map of E_0 for $\lambda_1 = -1$.

behavior of the discretized system. These inquiries are essential for understanding the implications of discretization and can significantly impact the design and analysis of discrete systems.

A. Stability analysis of equilibrium

The Jacobian matrix of system (5.5) is

$$M = \begin{pmatrix} 1 + \frac{\varsigma^q}{\Gamma(1+q)}\left(\frac{a(e-1)(2h+u-eu)v}{2(h+u-eu)^{\frac{3}{2}}} + \frac{(2-3u)u+m(2u-1)}{1+kv}\right) & \frac{\varsigma^q}{\Gamma(1+q)}\left(\frac{ua(e-1)}{\sqrt{h+u-eu}} + \frac{k(u-1)(u-m)}{(1+kv)^2}\right) \\ -\frac{\varsigma^q}{\Gamma(1+q)}\left(\frac{b(e-1)(2h+u-eu)v}{2(h+u-eu)^{\frac{3}{2}}}\right) & 1 + \frac{\varsigma^q}{\Gamma(1+q)}\left(-d - \frac{b(e-1)u}{\sqrt{h+u-eu}}\right) \end{pmatrix}. \quad (5.6)$$

The stability of a fixed point is determined by checking whether the eigenvalues of the Jacobian matrix lie within the unit circle.

Theorem 11:

(i) *E_0 is locally stable at Ω_{01}, locally unstable at Ω_{02} and a saddle point at Ω_{03};*
(ii) *E_1 is locally stable at Ω_{11}, locally unstable at Ω_{12} and a saddle point at Ω_{13};*
(iii) *E_2 is locally stable at Ω_{21}, locally unstable at Ω_{22} and a saddle point at Ω_{23}; and*
(iv) *if $|TrM_3| - 1 < DetM_3 < 1$, E_3 is locally asymptotically stable; if $|TrM_3| - 1 < DetM_3$ and $DetM_3 > 1$, E_3 is locally unstable; and if $|TrM_3| - 1 > DetM_3$, E_3 is a saddle point.*

Proof. The Jacobian matrix of the system at E_0 is

$$M_0 = \begin{pmatrix} 1 - \frac{m\varsigma^q}{\Gamma(1+q)} & 0 \\ 0 & 1 - \frac{d\varsigma^q}{\Gamma(1+q)} \end{pmatrix},$$

with eigenvalues $\lambda_1 = 1 - \frac{\varsigma^q m}{\Gamma(1+q)}$ and $\lambda_2 = 1 - \frac{d\varsigma^q}{\Gamma(1+q)}$. If m is a weak Allee effect, then $\lambda_1 > 1$; m has no Allee effect, then $\lambda_1 = 1$; m is a strong Allee effect, then $\lambda_1 < 1$. Thus, $-1 < \lambda_1 < 1$ holds when $m \in (0, 2\varsigma^{-q}\Gamma(1+q))$ is satisfied. Conversely, we obtain $\lambda_1 < -1$ for $m \in (2\varsigma^{-q}\Gamma(1+q), 1)$. Since $0 < d < 1$ is consistent with the strong Allee of m, the discussion will not be repeated here. Thus, for the stability analysis at E_0, the following conclusions are obtained, where $\Lambda = \varsigma^{-q}\Gamma(1+q)$:

(1) E_0 is locally asymptotically stable in $\Omega_{01} = \{(m, d, \varsigma, q) \in R^+ | m \in (0, 2\Lambda) \cap d \in (0, 2\Lambda)\}$;
(2) E_0 is locally unstable in $\Omega_{02} = \{(m, d, \varsigma, q) \in R^+ | \{m \in (2\Lambda, 1) \cup m \in (-1, 0)\} \cap d \in (2\Lambda, 1)\}$; and
(3) E_0 is a saddle point in $\Omega_{03} = \{(m, d, \varsigma, q) \in R^+ | \{m \in (2\Lambda, 1)$ or $m \in (-1, 0)\} \cap d \in (0, 2\Lambda)\} \cup \{(m, d, \varsigma, q) \in R^+ | m \in (0, 2\Lambda) \cap d \in (2\Lambda, 1)\}$.

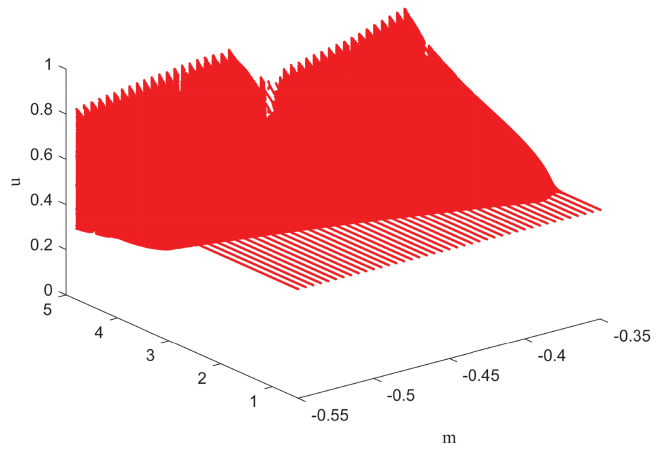

FIG. 14. Three-dimensional bifurcation diagram at bifurcation parameter ς.

The Jacobian matrix of the system at E_1 is

$$M_1 = \begin{pmatrix} 1 + \frac{\varsigma^q m(m-1)}{\Gamma(1+q)} & \frac{a(-1+e)\varsigma^q m}{\sqrt{h+m-em}\Gamma(1+q)} \\ 0 & 1 + \frac{\varsigma^q}{\Gamma(1+q)}\left(-d - \frac{b(-1+e)m}{\sqrt{h+m-em}}\right) \end{pmatrix},$$

with eigenvalues $\lambda_1 = 1 + \frac{\varsigma^q m(m-1)}{\Gamma(1+q)}$ and $1 + \frac{\varsigma^q}{\Gamma(1+q)}\left(-d - \frac{b(-1+e)m}{\sqrt{h+m-em}}\right)$. Due to the existence of E_1, $-1 < \lambda_1 < 1$ holds for $-2\Lambda < m(m-1)$. Similarly, $-1 < \lambda_2 < 1$ holds for $-2\Lambda < \frac{b(1-e)m}{\sqrt{h+m(1-e)}}$ < 0. The following conclusions are drawn for the stability case of E_1:

(1) E_1 is locally asymptotically stable in $\Omega_{11} = \{(m, d, \varsigma, q, b, e, h) \in R^+ | m(1-m) \in (0, 2\Lambda) \cap d \in (\frac{b(1-e)m}{\sqrt{h+m(1-e)}}, 2\Lambda)\}$;

(2) E_1 is locally unstable in $\Omega_{12} = \{(m, d, \varsigma, q, b, e, h) \in R^+ | m(1-m) \in (2\Lambda, 1) \cap \{d \in (0, \frac{b(1-e)m}{\sqrt{h+m(1-e)}})$ or $d \in (2\Lambda, 1)\}\}$; and

(3) E_1 is a saddle point in $\Omega_{13} = \{(m, d, \varsigma, q, b, e, h) \in R^+ | \{m(1-m) \in (0, 2\Lambda) \cap \{d \in (0, \frac{b(1-e)m}{\sqrt{h+m(1-e)}}) \cup d \in (2\Lambda, 1)\}\}$ or $\{d \in (\frac{b(1-e)m}{\sqrt{h+m(1-e)}}, 2\Lambda) \cap m(1-m) \in (2\Lambda, 1)\}\}$.

The Jacobian matrix of the system at E_2 is

$$M_2 = \begin{pmatrix} 1 + \frac{\varsigma^q(-1+m)}{\Gamma(1+q)} & \frac{\varsigma^q}{\Gamma(1+q)}\left(\frac{a(-1+e)}{\sqrt{1-e+h}}\right) \\ 0 & 1 + \frac{\varsigma^q}{\Gamma(1+q)}\left(-d - \frac{b(-1+e)}{\sqrt{1-e+h}}\right) \end{pmatrix},$$

with eigenvalues $\lambda_1 = 1 + \frac{\varsigma^q(-1+m)}{\Gamma(1+q)}$ and $\lambda_2 = 1 + \frac{\varsigma^q}{\Gamma(1+q)}\left(-d - \frac{b(-1+e)}{\sqrt{1-e+h}}\right)$. Since $m \in (-1, 1)$, i.e., $\lambda_1 < 1$ holds, if $1 - 2\Lambda \in (-1, 1)$, $-1 < \lambda_1 < 1$ holds for $m \in (-1, 1-2\Lambda)$. Conversely, $\lambda_1 < -1$ holds for $m \in (-1, 1-2\Lambda)$. If $1 < \Lambda$, then obtains $-1 < \lambda_1 < 1$ at $m \in (-1, 1)$. Similarly, $-1 < \lambda_2 < 1$ holds when $-2\Lambda < -d + \frac{b(1-e)}{\sqrt{1-e+h}} < 0$. Conversely when $-d + \frac{b(1-e)}{\sqrt{1-e+h}} > 0$ or $-d + \frac{b(1-e)}{\sqrt{1-e+h}} < -\Lambda$ is satisfied, we obtain $|\lambda_2| > 1$. The following conclusions are drawn for the stability case of E_2:

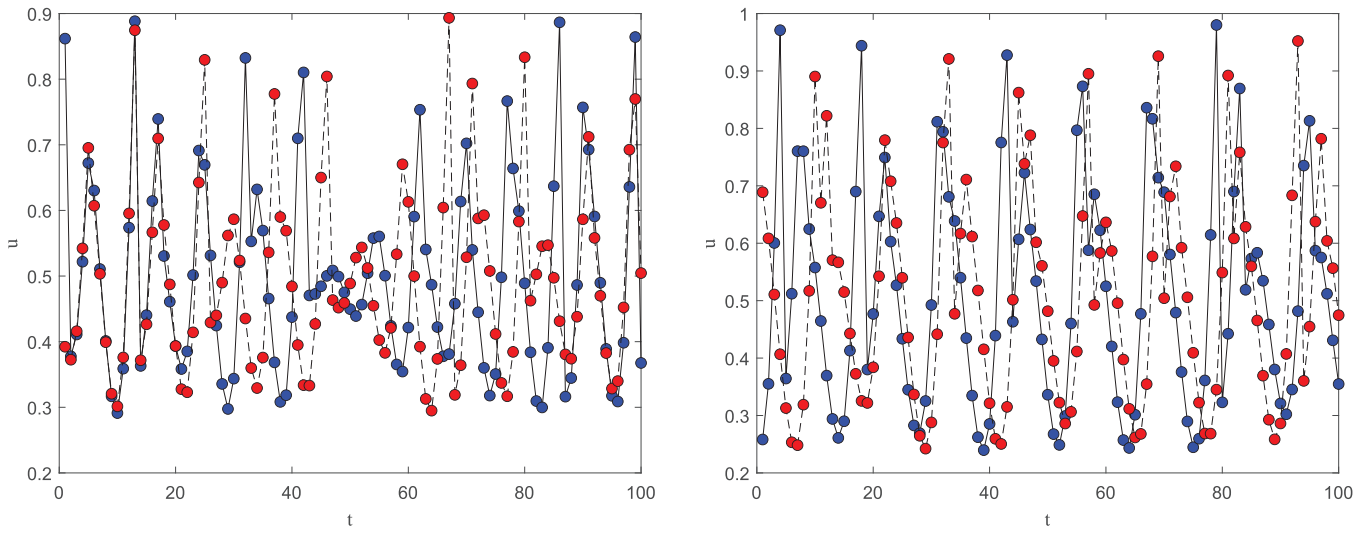

FIG. 15. (a) is the time series corresponding to Fig. 26(i), with initial points (0.49, 0.3) in blue and (0.5, 0.3) in red; (b) is the time series corresponding to Fig. 27(l), with initial points (0.4, 0.41) in blue, and (0.4, 0.4) in red.

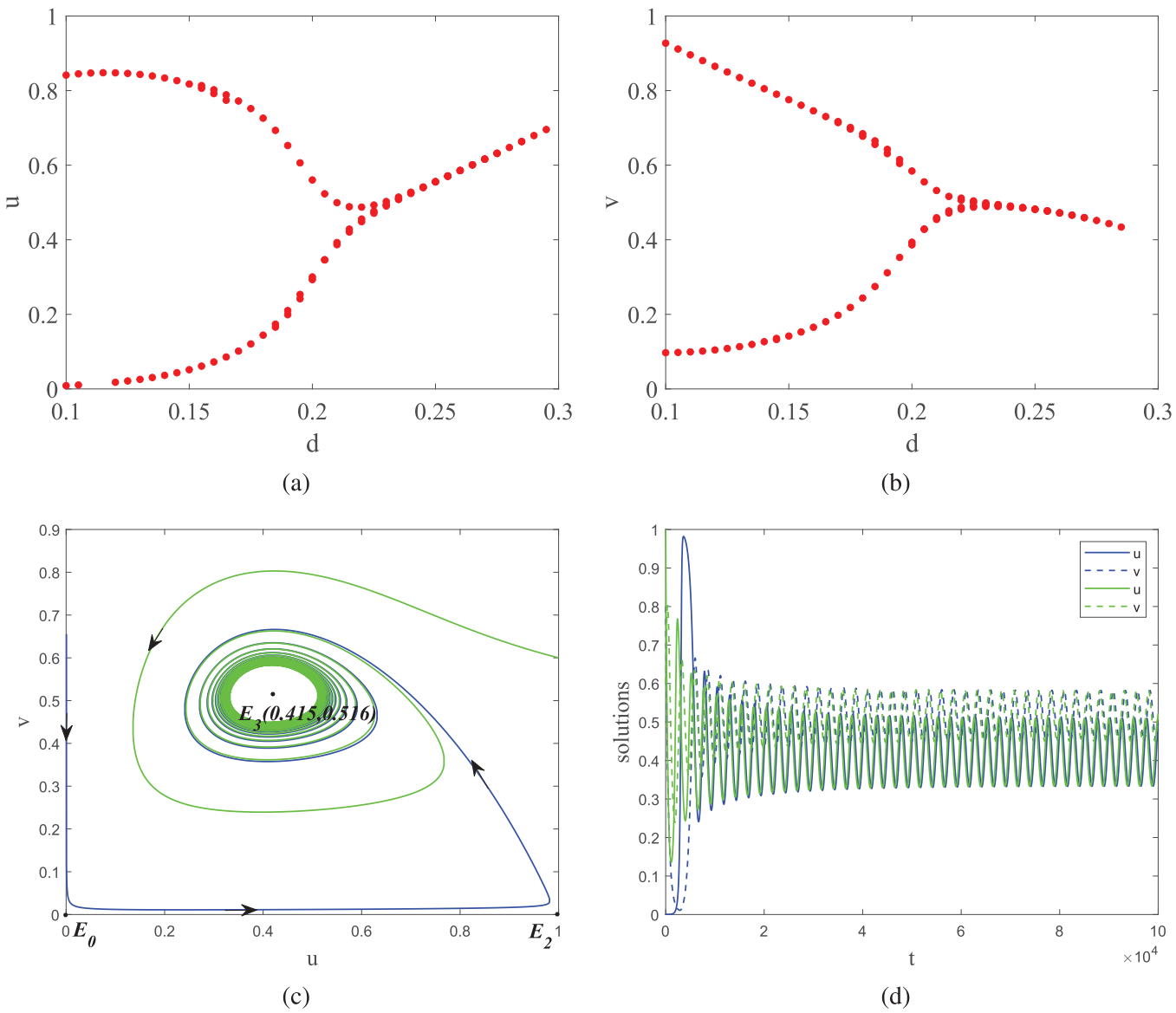

FIG. 16. (a) and (b) are bifurcation diagrams with parameter d for $m = -0.3, q = 0.98$; (c) and (d) are the phase diagram and solution curves of system (1.2) with initial value (0.001,0.6), (1,0.6), and $d = 0.2, m = -0.3$, respectively.

(1) E_2 is locally asymptotically stable in $\Omega_{11} = \{(m, d, \varsigma, q, b, e, h) \in R^+ | \Lambda \in (0, \frac{d}{2} - \frac{b(1-e)}{2\sqrt{1-e+h}}) \cap m \in (-1, 1-2\Lambda)\}$;

(2) E_2 is locally unstable in $\Omega_{12} = \{(m, d, \varsigma, q, b, e, h) \in R^+ | \Lambda > \frac{1}{2}$ or $\frac{d}{2} - \frac{b(1-e)}{2\sqrt{1-e+h}} < 0 \cup \{\Lambda \in (0, \frac{1}{2}) \cap m \in (-1, 1-2\Lambda)\}$ or $\{\Lambda \in (\frac{d}{2} - \frac{b(1-e)}{2\sqrt{1-e+h}}, \frac{1}{2}) \cap m \in (1-2\Lambda, 1)\}\}$; and

(3) E_2 is a saddle point in $\Omega_{13} = \{(m, d, \varsigma, q, b, e, h) \in R^+ | \{\Lambda \in (\frac{d}{2} - \frac{b(1-e)}{2\sqrt{1-e+h}}, \frac{1}{2}) \cap m \in (-1, 1-2\Lambda)\}$ or $\{\Lambda \in (0, \frac{1}{2}) \cap \frac{d}{2} - \frac{b(1-e)}{2\sqrt{1-e+h}} < 0 \cap m \in (1-2\Lambda, 1)\}$ or $\{\Lambda \in (0, \frac{d}{2} - \frac{b(1-e)}{2\sqrt{1-e+h}}) \cap m \in (1-2\Lambda, 1)\}\}$.

The Jacobian matrix of the system at E_3 is

$$M_3 = \begin{pmatrix} M_{11} & M_{12} \\ M_2 & M_{22} \end{pmatrix}, \tag{5.7}$$

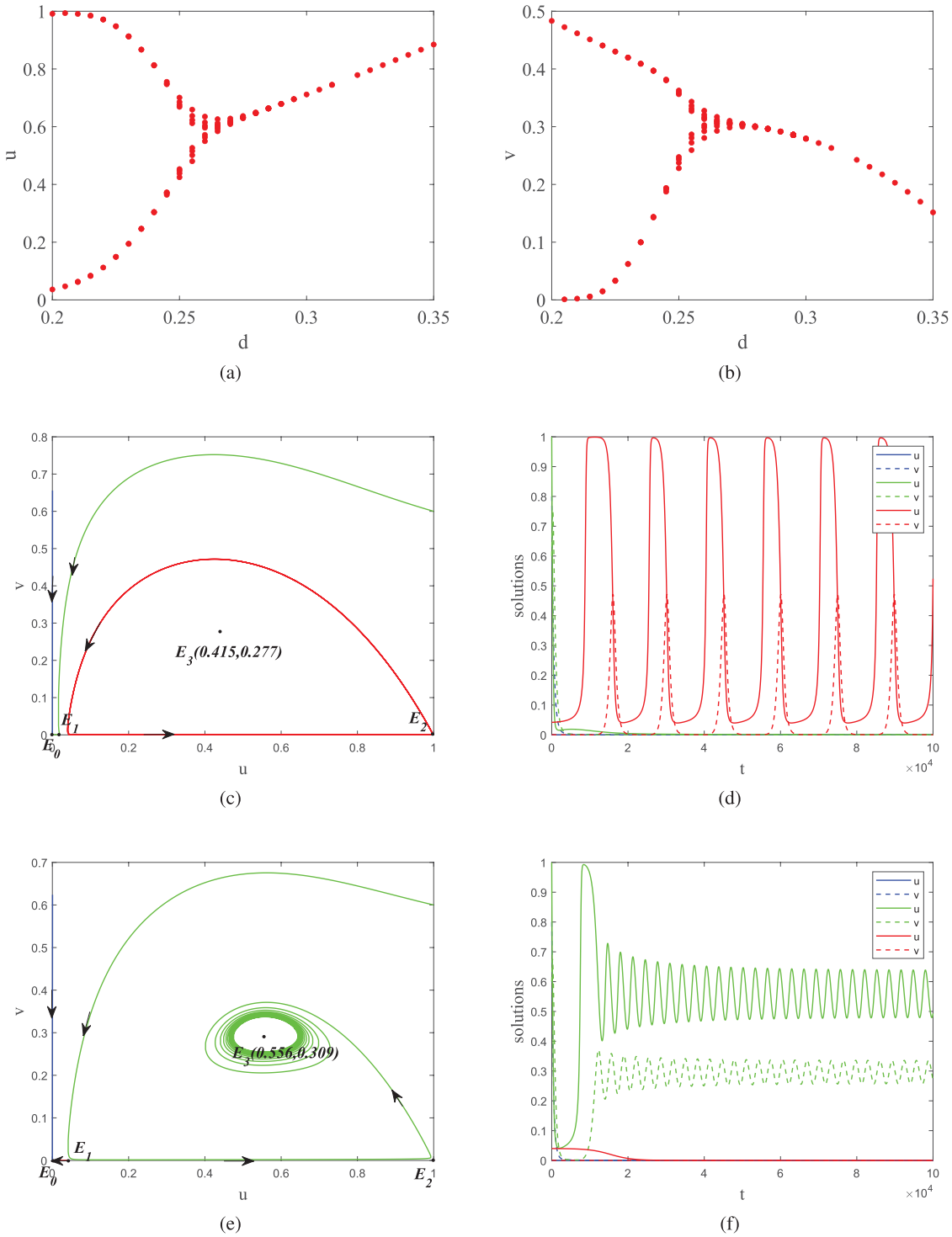

FIG. 17. (a) and (b) are bifurcation diagrams with parameter d for $m = 0.04, q = 0.98$; (c) and (d) are the phase diagram and solution curves of system (1.2) with initial values $(0.001, 0.6)$ in blue, $(1, 0.6)$ in green, $(0.041, 0.001)$ in red and $d = 0.2, m = 0.04$, respectively; (e) and (f) are the phase diagram and solution curves of system (1.2) with initial values $(0.001, 0.6)$ in blue, $(1, 0.6)$ in green, and $(0.04, 0.001)$ in red and $d = 0.25, m = 0.04$, respectively.

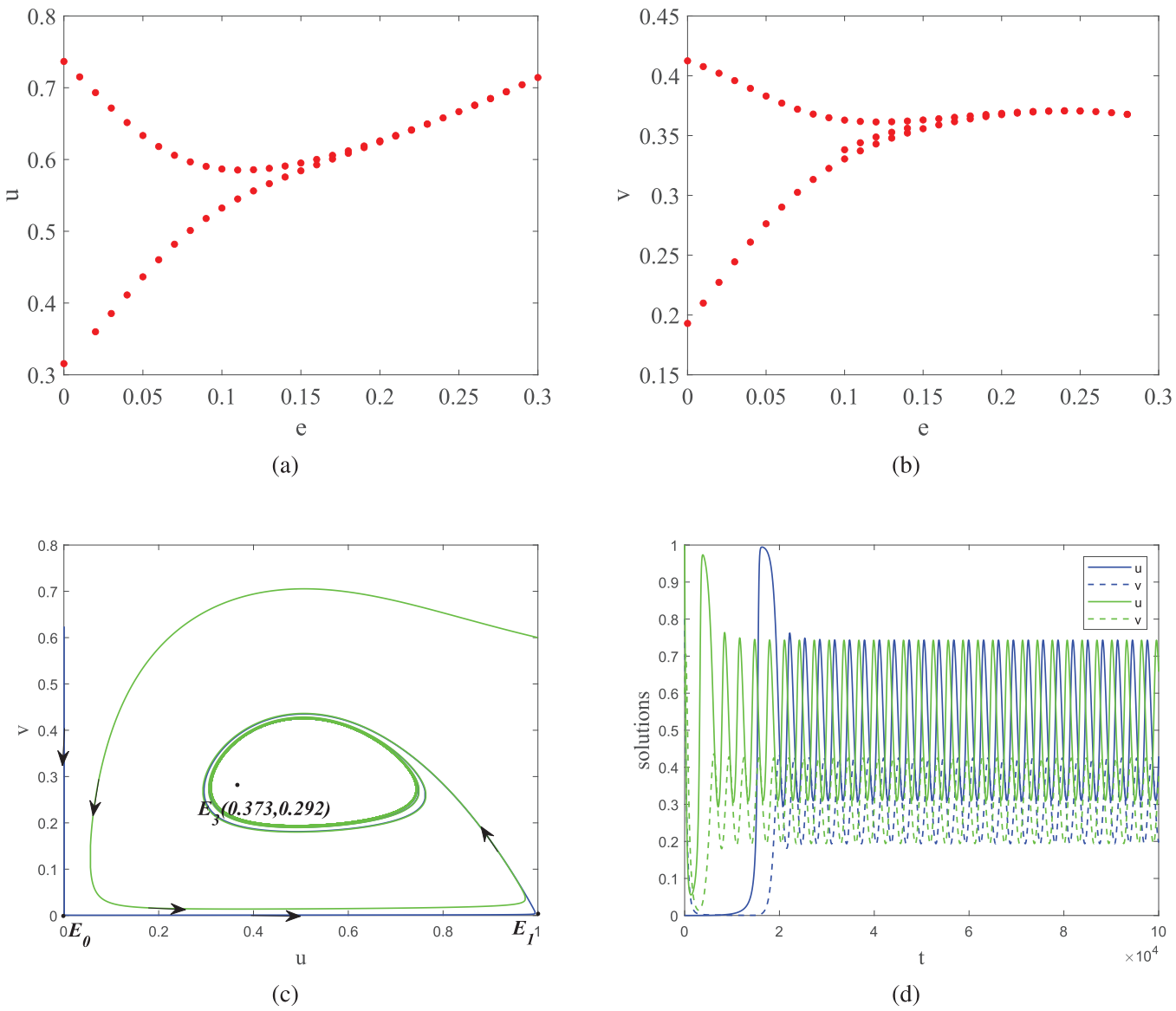

FIG. 18. (a) and (b) are bifurcation diagrams with parameter e for $m = -0.05$, $q = 0.98$; (c) and (d) are the phase diagram and solution curves of system (1.2) with initial value $(0.001, 0.6)$ in blue, and $(1, 0.6)$ in green and $e = 0, m = -0.05$, respectively.

where

$$M_{11} = 1 + \frac{\varsigma^q a(-1+e)^2 u_3 v_3}{2(h+u_3-eu_3)^{3/2}} + \frac{(1+m-2u_3)u_3}{1+kv_3\Gamma(1+q)},$$

$$M_{12} = -\frac{\varsigma^q b(-1+e)(2h+u-eu)v}{2(h+u-eu)^{\frac{3}{2}}\Gamma(1+q)},$$

$$M_{21} = -\frac{\varsigma^q b(-1+e)(2h+u_3-eu_3)v_3}{2(h+u_3-eu_3)^{\frac{3}{2}}\Gamma(1+q)},$$

$$M_{22} = 1.$$

As a comparison with (4.4), we rewrite (5.7) as (5.8)

$$M_3 = \begin{pmatrix} 1+\frac{\varsigma^q J_{11}}{\Gamma(1+q)} & \frac{\varsigma^q J_{12}}{\Gamma(1+q)} \\ \frac{\varsigma^q J_{21}}{\Gamma(1+q)} & 1 \end{pmatrix}. \tag{5.8}$$

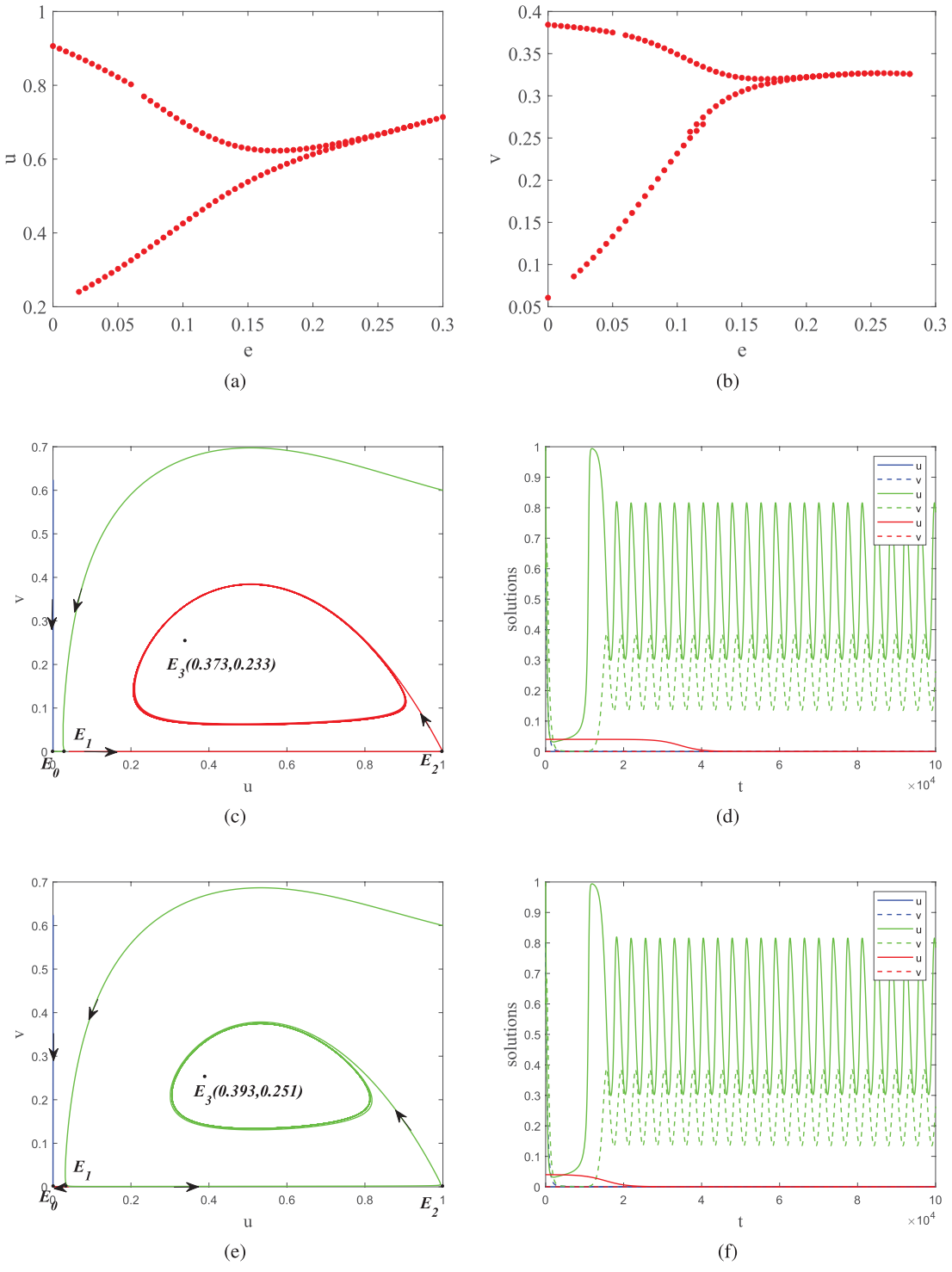

FIG. 19. (a) and (b) are bifurcation diagrams with parameter e for $m = 0.04, q = 0.98$; (c) and (d) are the phase diagram and solution curves of system (1.2) with initial values $(0.001, 0.6)$ in blue, and $(1, 0.6)$ in green, $(0.041, 0.001)$ in red and $e = 0, m = 0.04$, respectively; (e) and (f) are the phase diagram and solution curves of system (1.2) with initial values $(0.001, 0.6)$ in blue, $(1, 0.6)$ in green, and $(0.04, 0.001)$ in red and $e = 0.05, m = 0.04$, respectively.

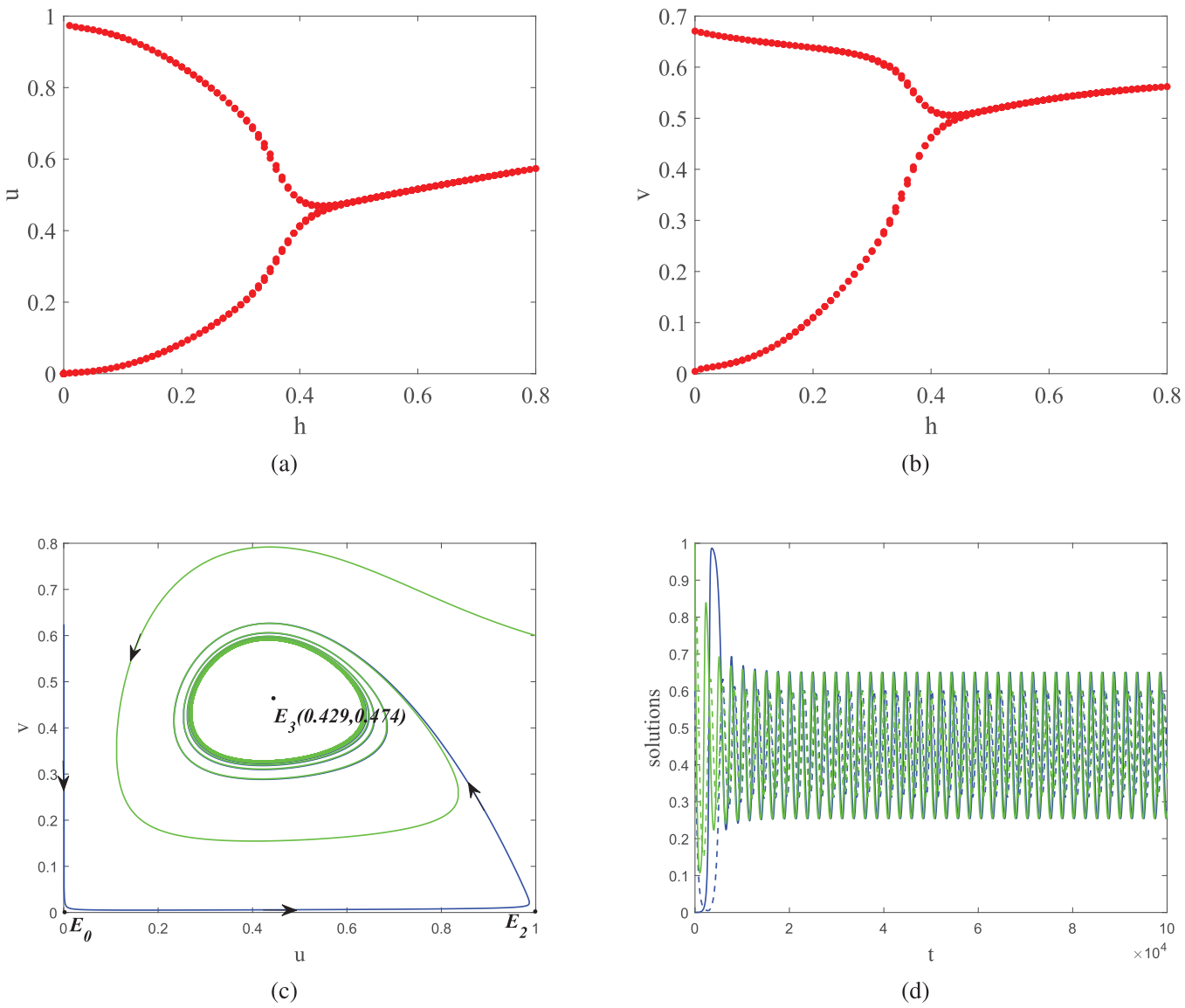

FIG. 20. (a) and (b) are bifurcation diagrams with parameter h for $m = -0.3, q = 0.98$; (c) and (d) are the phase diagram and solution curves of system (1.2) with initial value $(0.001, 0.6)$ in blue, and $(1, 0.6)$ in green and $h = 0.35, m = -0.3$, respectively.

Thus, the characteristic equation for E_3 is $F(\lambda) = \lambda^2 - TrM_3\lambda + DetM_3$, where

$$TrM_3 = 2 + \frac{\varsigma^q J_{11}}{\Gamma(1+q)},$$

$$DetM_3 = 1 - \frac{\varsigma^{2q} J_{12} J_{21}}{\Gamma(1+q)^2} + \frac{\varsigma^q J_{11}}{\Gamma(1+q)}.$$

All eigenvalues λ of M_3 satisfy that $|\lambda| < 1$ if and only if $|TrM_3| - 1 < DetM_3 < 1$. Assume that $|TrM_3| - 1 = DetM_3$,

(a) if $TrM_3 > 0$, then the eigenvalues of M_3 are $\lambda = 1$ and $\lambda = DetM_3$; and
(b) if $TrM_3 < 0$, then the eigenvalues of M_3 are $\lambda = -1$ and $\lambda = -DetM_3$.

Assume that $|TrM_3| - 1 \leqslant DetM_3 = 1$, then the eigenvalues of M_3 are $\lambda = e^{\pm i\omega}$, where $\omega = \cos^{-1}\left(\frac{TrM_3}{2}\right)$. From Definition 3, we can obtain the type of equilibrium point for E_3,

(1) if $|TrM_3| - 1 < DetM_3 < 1$, E_3 is locally asymptotically stable;

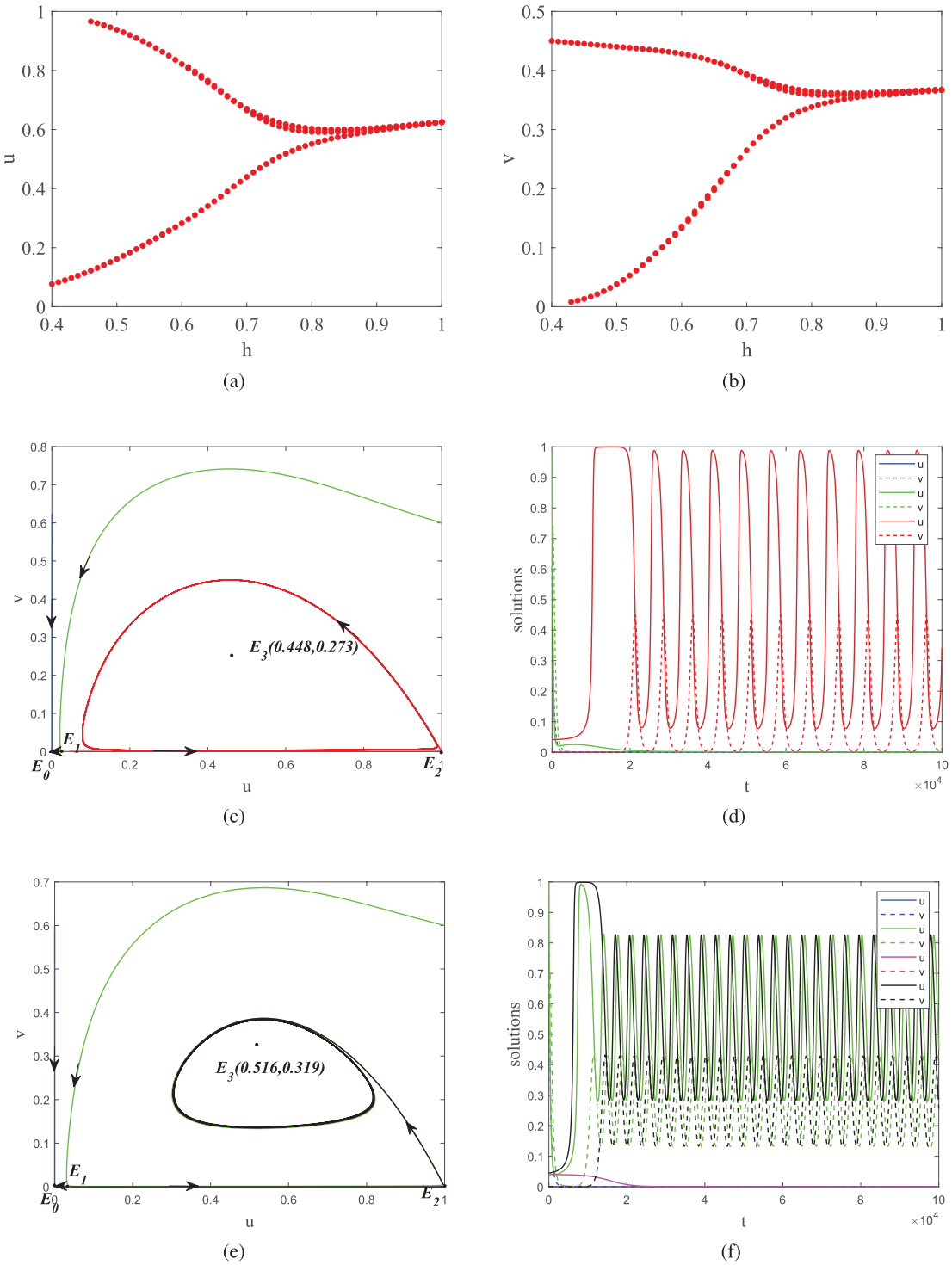

FIG. 21. (a) and (b) are bifurcation diagrams with parameter h for $m = 0.04, q = 0.98$; (c) and (d) are the phase diagram and solution curves of system (1.2) with initial values (0.001,0.6) in blue, (1,0.6) in green, and (0.041, 0.001) in red and $h = 0.4$, $m = 0.04$, respectively; (e) and (f) are the phase diagram and solution curves of system (1.2) with initial values (0.001,0.6) in blue, (1, 0.6) in green, (0.04, 0.001) in red, and (0.041, 0.001) in black and $h = 0.6, m = 0.04$, respectively.

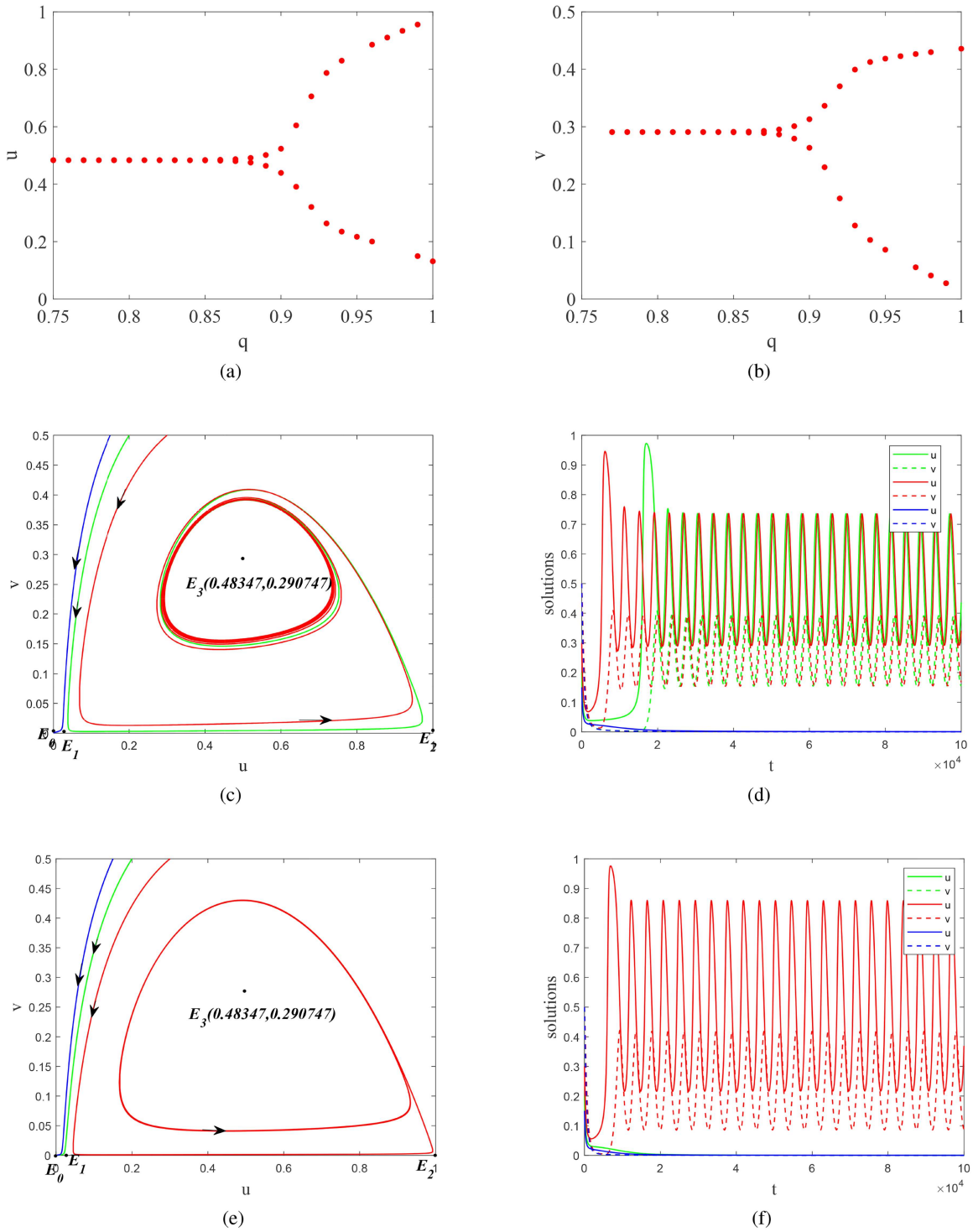

FIG. 22. (a) and (b) are bifurcation diagrams with parameter q for $m = 0.04$; (c) and (d) are the phase diagram and solution curves of system (1.2) with initial value $(0.17, 0.5)$ in blue, $(0.2, 0.5)$ in green, and $(0.3, 0.5)$ in red and $q = 0.91$, $m = 0.04$, respectively. (e) and (f) are the phase diagram and solution curves of system (1.2) with initial value $(0.17, 0.5)$ in blue, $(0.2, 0.5)$ in green, and $(0.3, 0.5)$ in red and $q = 0.95$, $m = 0.04$, respectively.

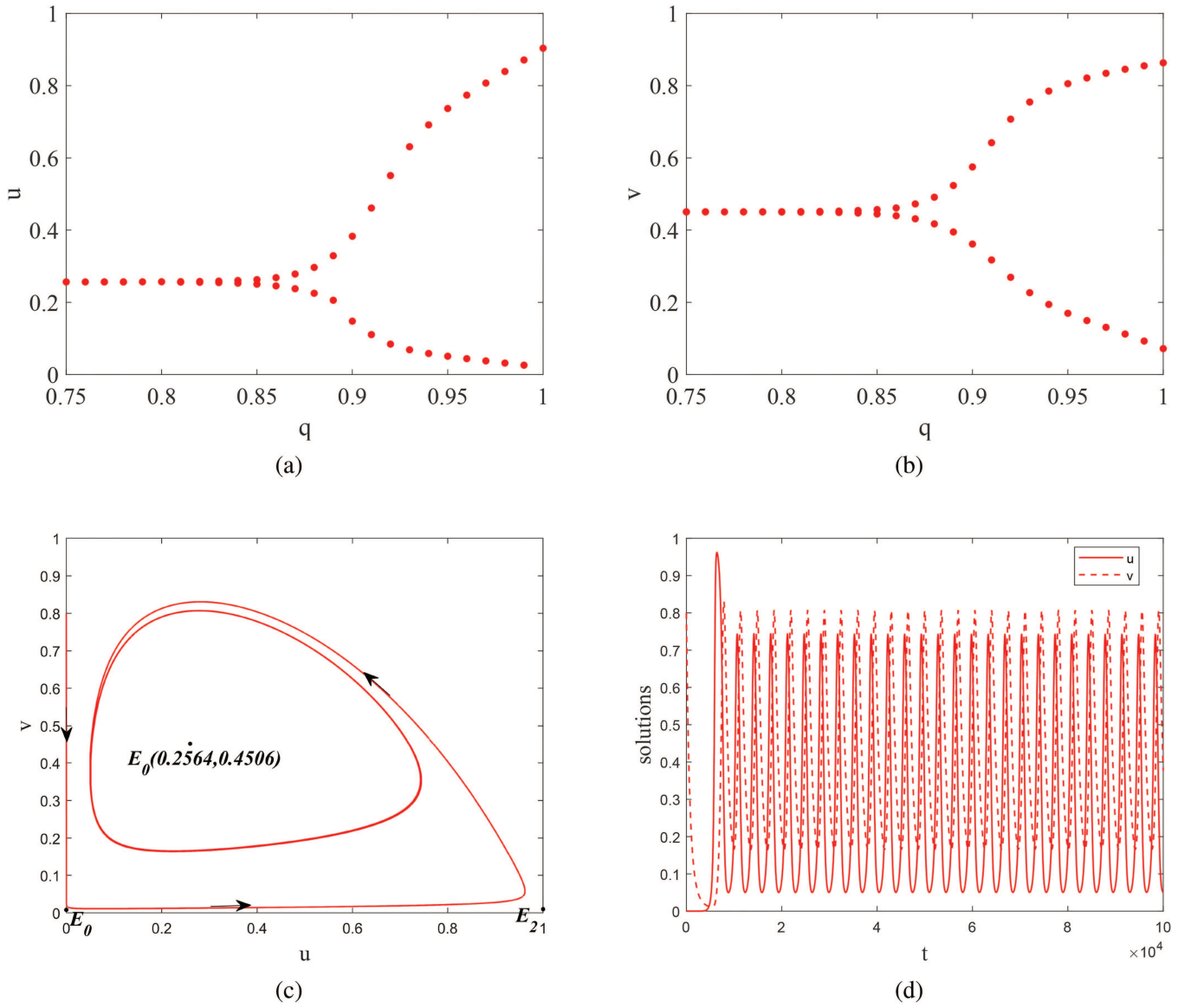

FIG. 23. (a) and (b) are bifurcation diagrams with parameter ς for $m = 0.04$; (c) and (d) are the phase diagram and solution curves of the system (1.2) with initial value (0.001, 0.6) in red and $q = 0.95, m = -0.3$, respectively.

(2) if $|TrM_3| - 1 < DetM_3$ and $DetM_3 > 1$, E_2 is locally unstable; and
(3) if $|TrM_3| - 1 > DetM_3$, E_2 is a saddle point.

□

Remark 6: *The local stability analysis of the discrete system (5.5) is a more complex task compared to its continuous counterpart due to the impact of the step size ς. However, when $\varsigma = \sqrt[q]{2\Gamma(1+q)m^{-1}}$, the equilibrium point stability remains the same for both systems. In contrast, the stability of the equilibrium point in the discrete case is considerably influenced by the choice of ς. Specifically, when $0 < \varsigma < \sqrt[q]{2\Gamma(1+q)m^{-1}}$, the stability domain of the discrete system is smaller than that of the continuous system. As a result, the selection of step ς in numerical simulations becomes critical for obtaining accurate results.*

Remark 7: *The influence of ς on the stability of E_0 is studied in Theorem 11, which reveal that the stability of E_0 depends on ς. If $\Lambda > \frac{1}{2}$, then the stability of E_0 is consistent with the continuous case. On the other hand, if $\Lambda \leqslant \frac{1}{2}$, i.e., $0 < \varsigma < \sqrt[q]{2\Gamma(1+q)m^{-1}}$, the stability region becomes narrower. To aid in choosing an appropriate step*

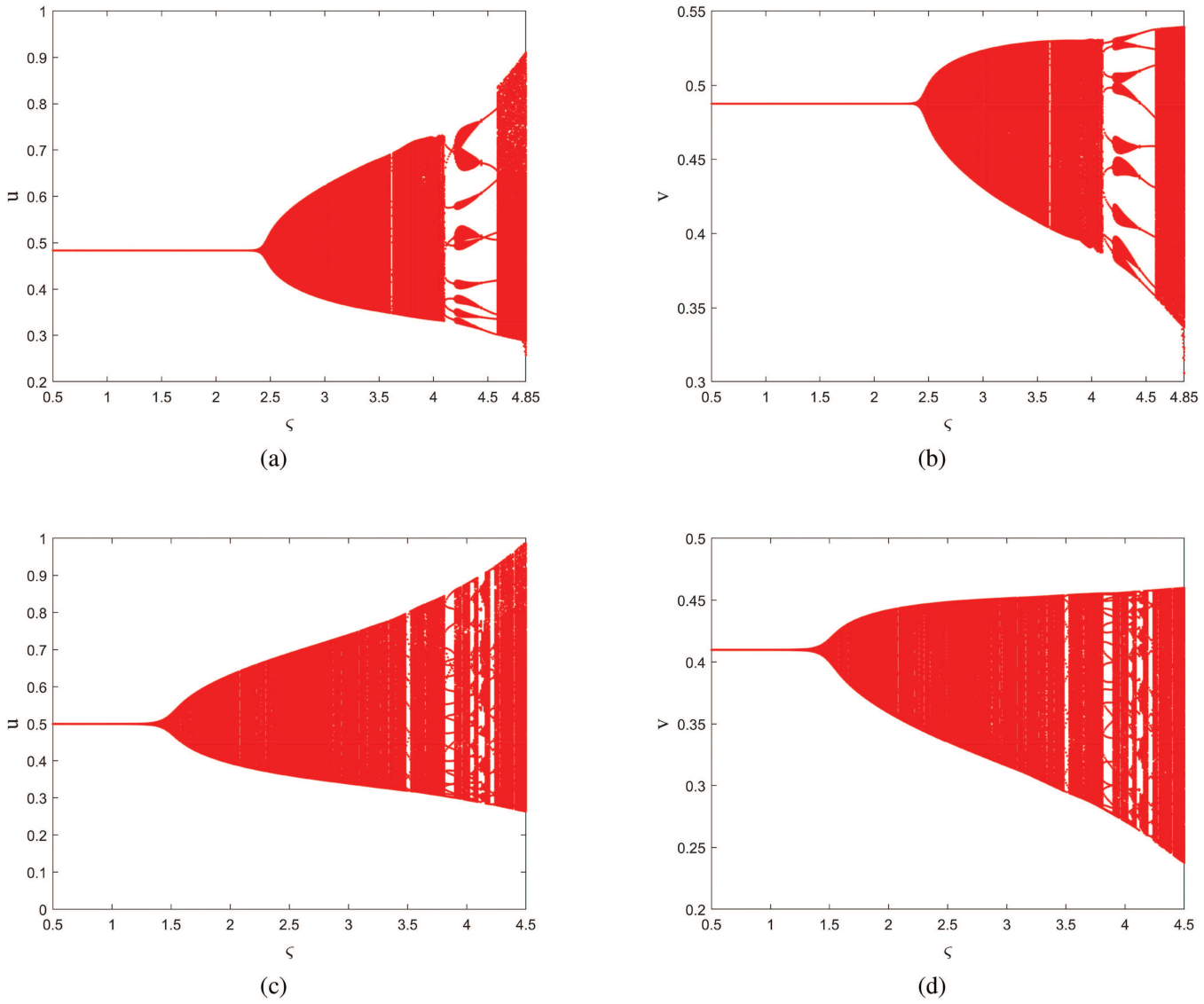

FIG. 24. (a) and (b) are bifurcation diagrams with parameter ς for $m = -0.5, q = 0.98$; (c) and (d) are bifurcation diagrams with parameter ς for $m = -0.35, q = 0.98$.

and adjusting the stability of E_0, Fig. 13 shows the Λ density map for ς and q, with the white curve indicating $\Lambda = \frac{1}{2}$. Figure 13(b) illustrates the impact of Λ on E_0 by taking λ_1 as an example. The results indicate that the stability of E_0 in the discrete case is highly influenced by step size ς and order q, which allows for flexible adjustment of the system solution's overall trend.

Furthermore, the stability of E_1, E_2, and E_3 is also affected by ς. Notably, the existence of E_1 is related to the strength of Allee, and the stability of E_1 and E_2 depends on the presence of E_3. For example, when E_3 exists, the stability of E_2 disappears. These findings highlight the importance of considering the impact of the step size on the stability of equilibrium points in discrete fractional-order systems.

B. Bifurcation analysis

In this section, we investigate Neimark–Sacker bifurcation at $E_3(x_3, y_3)$. Consider system (5.5) where the multipliers of the Jacobian matrix at $E_3(u_3, v_3)$ are two complex conjugate roots of modulus 1. Assume that $Tr^2M_3 - 4DetM_3 < 0$, that is,

$$\frac{\varsigma^{2q}\left(J_{11}^2 + 4J_{12}J_{21}\right)}{\Gamma(q+1)^2} < 0. \tag{5.9}$$

Due to the roots of $F(\lambda)$ are conjugate complex numbers $\lambda_{1,2} = \frac{Tr \pm i\sqrt{4Det - Tr^2}}{2}$ with $|\lambda_{1,2}| = 1$, we can obtain

$$\tilde{\varsigma} = \sqrt[q]{\frac{J_{11}\Gamma(q+1)}{J_{12}J_{21}}}. \tag{5.10}$$

From $-2 < Tr < 2$ and $Tr \neq 0, -1$, we get $\lambda_{1,2}^m \neq 1$ for all $m = 1, 2, 3, 4$, hence $\lambda_{1,2}$ is not at the intersection of the unit circle and the coordinate axis when the following equation is satisfied:

$$-4 < \frac{J_{11}\varsigma^q}{\Gamma(q+1)} < 0, \text{ and } \varsigma \neq \left(\frac{\Gamma(q+1)}{J_{11}}\right)^{\frac{1}{q}}, \varsigma \neq \left(\frac{3\Gamma(q+1)}{2J_{11}}\right)^{\frac{1}{q}}. \tag{5.11}$$

Assume that

$$S_3 = \left\{(a, b, d, e, h, k, \varsigma, q) \in R_+^8 : (5.9) - (5.11) \text{ are satisfied}\right\}.$$

The unique positive equilibrium point $E_3(u_3, v_3)$ of system (5.5) undergoes Neimark–Sacker bifurcation when it changes in the neighborhood of $\Omega_{NSB} = S_1 \cap S_3$.

Next, we further analyze the approximate expressions for the stability of the Neimark–Sacker bifurcation, the direction of the bifurcation, and the invariant curve resulting from the bifurcation. Let $\tilde{\varsigma} = \varsigma + \varepsilon$ and choosing the parameters $(a, b, d, e, h, k, \varsigma, q)$ in an arbitrary value from the set Ω_{NSB}, we consider the transformations $x = u - u_3, y = v - v_3$, then system (5.5) is transferred into the following form:

$$\begin{pmatrix} x \\ y \end{pmatrix} \to \begin{pmatrix} \theta_1 & \theta_2 \\ \theta_3 & 1 \end{pmatrix} \begin{pmatrix} x \\ y \end{pmatrix} + \begin{pmatrix} f(x,y) \\ g(x,y) \end{pmatrix}, \tag{5.12}$$

where

$$f(x,y) = a_{20}x^2 + a_{11}xy + a_{02}y^2 + a_{30}x^3 + a_{21}x^2y + a_{12}xy^2 + a_{03}y^3 + O\left((|x| + |y|)^4\right),$$
$$g(x,y) = b_{20}x^2 + b_{11}xy + b_{02}y^2 + b_{30}x^3 + b_{21}x^2y + b_{12}xy^2 + b_{03}y^3 + O\left((|x| + |y|)^4\right).$$

The characteristic equation of the Jacobian matrix of the linearized system of (5.12) evaluated at the equilibrium $(0, 0)$ can be written as follows:

$$\theta_1 = 1 + \frac{\tilde{\varsigma}^q a(-1+e)^2 u_3 v_3}{2(h + u_3 - eu_3)^{3/2}} + \frac{\tilde{\varsigma}^q(1 + m - 2u_3)u_3}{(1 + kv_3)\Gamma(1+q)}, \quad \theta_2 = -\frac{\tilde{\varsigma}^q b(-1+e)(2h + u - eu_3)v_3}{2(h + u - eu_3)^{\frac{3}{2}}\Gamma(1+q)},$$

$$\theta_3 = -\frac{\tilde{\varsigma}^q b(-1+e)(2h + u_3 - eu_3)v_3}{2(h + u_3 - eu_3)^{\frac{3}{2}}\Gamma(1+q)},$$

$$a_{20} = \frac{\tilde{\varsigma}^q(m - 3u_3 + 1)}{(kv_3 + 1)\Gamma(q+1)} + \frac{a(e-1)^2 v_3 \tilde{\varsigma}^q(4h + u_3 - eu_3) + a(e-1)^2 k v_3^2 \tilde{\varsigma}^q(4h + u_3 - eu_3)}{8(kv_3 + 1)\Gamma(q+1)(h + u_3 - eu_3)^{\frac{5}{2}}},$$

$$a_{11} = \frac{\tilde{\varsigma}^q}{2\Gamma(q+1)}\left(\frac{a(e-1)(2h + u_3 - eu_3)}{(h + u_3 - eu_3)^{3/2}} + \frac{2k(-2mu_3 + m + u_3(3u_3 - 2))}{(kv_3 + 1)^2}\right), \quad a_{02} = \frac{k^2(u_3 - 1)u_3\tilde{\varsigma}^q(m - u_3)}{(kv_3 + 1)^3\Gamma(q+1)},$$

$$a_{30} = \frac{-\tilde{\varsigma}^q}{kv_3\Gamma(q+1)} + \frac{a(e-1)^3 v_3 \tilde{\varsigma}^q(6h + u_3 - eu_3) + a(e-1)^3 k v_3^2 \tilde{\varsigma}^q(6h + u_3 - eu_3)}{16(kv_3 + 1)\Gamma(q+1)(-eu_3 + h + u_3)^{\frac{7}{2}}},$$

$$a_{21} = \Phi_1 + \Phi_2 v_3 + \frac{k\Phi_2}{2}v_3, \quad a_{12} = \frac{k^2\tilde{\varsigma}^q(m(2u_3 - 1) + u_3(2 - 3u_3))}{(kv_3 + 1)^3\Gamma(q+1)},$$

$$a_{03} = -\frac{k^3(u_3 - 1)u_3\tilde{\varsigma}^q(m - u_3)}{(kv_3 + 1)^4\Gamma(q+1)},$$

$$\Phi_1 = \frac{\tilde{\varsigma}^q\left(a(e-1)^2(4h + u_3 - eu_3) - 8k(m - 3u_3 + 1)(h + u_3 - eu_3)^{\frac{5}{2}}\right)}{8(kv_3 + 1)^2\Gamma(q+1)(-eu_3 + h + u_3)^{\frac{5}{2}}},$$

$$\Phi_2 = \frac{a(e-1)^2 k\tilde{\varsigma}^q(4h + u_3 - eu_3)}{4(kv_3 + 1)^2\Gamma(q+1)(-eu_3 + h + u_3)^{\frac{5}{2}}},$$

$$b_{21} = -\frac{b(e-1)^2\tilde{\varsigma}^q(4h + u_3 - eu_3)}{8\Gamma(q+1)(-eu_3 + h + u_3)^{\frac{5}{2}}},$$

$$b_{12} = b_{02} = b_{03} = b_{30} = 0.$$

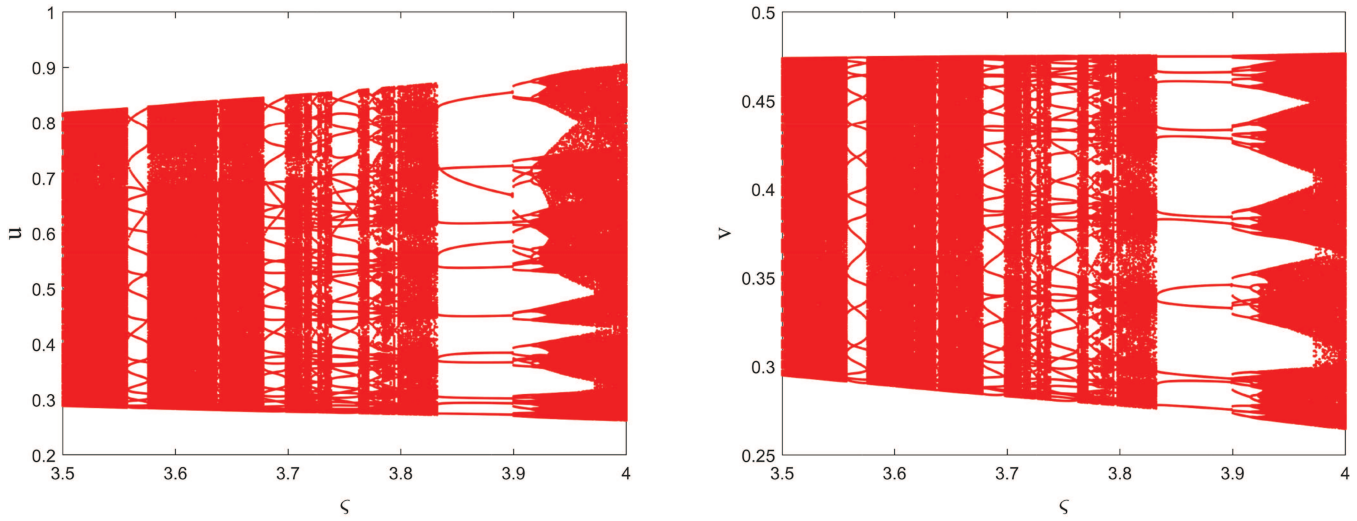

FIG. 25. Figure corresponding to the detail of Figs. 24(c) and 24(d) in (0.35, 4).

In order to obtain the normal form of (5.12) at $\varepsilon = 0$, we take $\alpha = \frac{Tr(0)}{2}, \beta = \frac{1}{2}\sqrt{4Det(0) - Tr^2(0)}$ and consider the following transformation:

$$\begin{pmatrix} x \\ y \end{pmatrix} = \begin{pmatrix} \theta_2 & 0 \\ \alpha - \theta_1 & -\beta \end{pmatrix} \begin{pmatrix} \omega_1 \\ \omega_2 \end{pmatrix}. \tag{5.13}$$

Under transformation (5.13), the normal form of (5.12) can be written as

$$\begin{pmatrix} \omega_1 \\ \omega_2 \end{pmatrix} \to \begin{pmatrix} \alpha & -\beta \\ \beta & \alpha \end{pmatrix} \begin{pmatrix} \omega_1 \\ \omega_2 \end{pmatrix} + \begin{pmatrix} \tilde{f}(\omega_1, \omega_2) \\ \tilde{g}(\omega_1, \omega_2) \end{pmatrix},$$

where

$$\begin{aligned}
\tilde{f}(\omega_1, \omega_2) &= \frac{a_{20}}{\theta_2}x^2 + \theta_1\theta_2 xy + \frac{a_{02}}{\theta_2}y^2 + \frac{a_{30}}{\theta_2}x^3 + \frac{a_{21}}{\theta_2}x^2y + \frac{a_{12}}{\theta_2}xy^2 \\
&\quad + \frac{a_{03}}{\theta_2}y^3 + O\left((|\omega_1| + |\omega_2|)^4\right), \\
\tilde{g}(\omega_1, \omega_2) &= \left(\frac{a_{20}(\alpha - \theta_1)}{\beta\theta_2} - \frac{b_{20}}{\beta}\right)x^2 + \left(\frac{\theta_1(\alpha - \theta_1)}{\beta\theta_2} - \frac{b_{11}}{\beta}\right)xy \\
&\quad + \left(\frac{a_{02}(\alpha - \theta_1)}{\beta\theta_2} - \frac{b_{02}}{\beta}\right)y^2 + \left(\frac{a_{30}(\alpha - \theta_1)}{\beta\theta_2} - \frac{b_{30}}{\beta}\right)x^3 \\
&\quad + \left(\frac{a_{21}(\alpha - \theta_1)}{\beta\theta_2} - \frac{b_{21}}{\beta}\right)x^2y + \left(\frac{a_{12}(\alpha - \theta_1)}{\beta\theta_2} - \frac{b_{12}}{\beta}\right)xy^2 \\
&\quad + \left(\frac{a_{03}(\alpha - \theta_1)}{\beta\theta_2} - \frac{b_{03}}{\beta}\right)y^3 + O\left((|\omega_1| + |\omega_2|)^4\right),
\end{aligned}$$

$x = \theta_2\omega_1$ and $y = (\alpha - \theta_1)\omega_1 - \beta\omega_2$. Next, we define the following nonzero real number:

$$\begin{aligned}
L = \Big(\Big[&- \mathrm{Re}\left(\frac{(1 - 2\lambda_1)\lambda_2^2}{1 - \lambda_1}\xi_{20}\xi_{11}\right) - \frac{1}{2}|\xi_{11}|^2 - |\xi_{02}|^2 \\
&+ \mathrm{Re}\left(\lambda_2\xi_{21}\right)\Big]\Big)_{\varepsilon=0},
\end{aligned}$$

where

$$\begin{aligned}
\xi_{20} &= \frac{1}{8}\left[\tilde{f}_{\omega_1\omega_1} - \tilde{f}_{\omega_2\omega_2} + 2\tilde{g}_{\omega_1\omega_2} + i\left(\tilde{g}_{\omega_1\omega_1} - \tilde{g}_{\omega_2\omega_2} - 2\tilde{f}_{\omega_1\omega_2}\right)\right], \\
\xi_{11} &= \frac{1}{4}\left[\tilde{f}_{\omega_1\omega_1} + \tilde{f}_{\omega_1\omega_2} + i\left(\tilde{g}_{\omega_1\omega_1} + \tilde{g}_{\omega_2\omega_2}\right)\right], \\
\xi_{02} &= \frac{1}{8}\left[\tilde{f}_{\omega_1\omega_1} - \tilde{f}_{\omega_2\omega_2} - 2\tilde{g}_{\omega_1\omega_2} + i\left(\tilde{g}_{\omega_1\omega_1} - \tilde{g}_{\omega_2\omega_2} + 2\tilde{f}_{\omega_1\omega_2}\right)\right], \\
\xi_{21} &= \frac{1}{16}\Big[\tilde{f}_{\omega_1\omega_1\omega_1} + \tilde{f}_{\omega_1\omega_2\omega_2} + \tilde{g}_{\omega_1\omega_1\omega_2} + \tilde{g}_{\omega_2\omega_2\omega_2} \\
&\quad + i\left(\tilde{g}_{\omega_1\omega_1\omega_1} + \tilde{g}_{\omega_1\omega_2\omega_2} - \tilde{f}_{\omega_1\omega_1\omega_2} - \tilde{f}_{\omega_2\omega_2\omega_2}\right)\Big].
\end{aligned}$$

Theorem 12: *Assume that* $(a, b, d, e, h, k, \varsigma, q) \in \Omega_{NSB}$ *holds and* $L \neq 0$, *then system* (5.5) *undergoes the Neimark–Sacker bifurcation at the unique positive equilibrium point* $E_3(u_3, v_3)$ *when the parameter* ε *varies in a small neighborhood of* $\tilde{\varsigma} = \sqrt[q]{\frac{J_{11}\Gamma(q+1)}{J_{12}J_{21}}}$. *Furthermore, if* $L < 0$, *then an attracting invariant closed curve bifurcates from the equilibrium point for* $\varsigma > \tilde{\varsigma}$, *and if* $L > 0$, *then a repelling invariant closed curve bifurcates from the equilibrium point for* $0 < \varsigma < \tilde{\varsigma}$.

Remark 8: *This section focuses on considering the effect of step* ς *on the discrete system, for which we perform a full bifurcation analysis and illustrate its bifurcation behavior under weak effects via Fig. 24. It is noteworthy that the bifurcation characteristics of* ς *may*

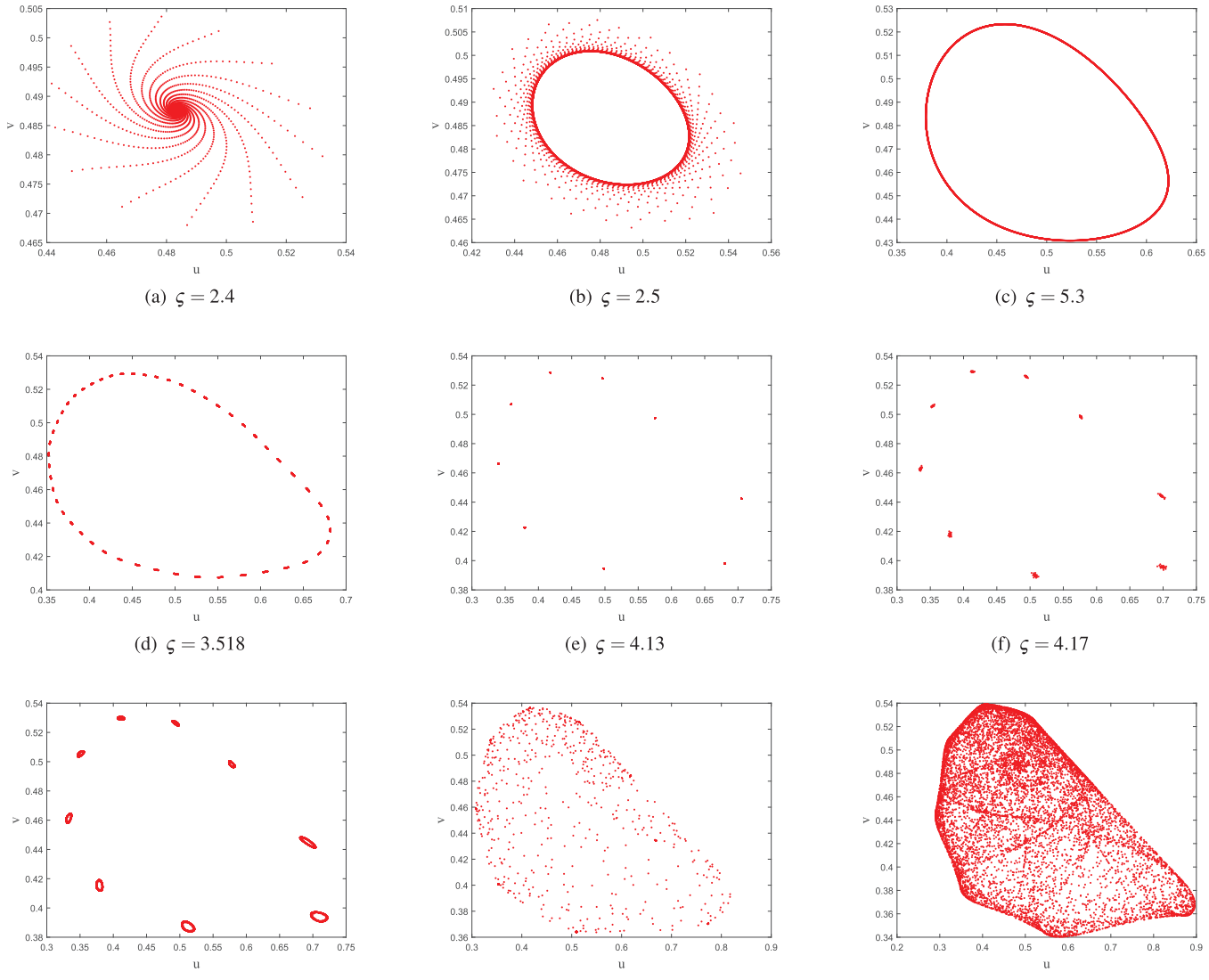

FIG. 26. Phase diagrams corresponding to Figs. 24(a) and 24(d). (a) $\varsigma = 2.4$, (b) $\varsigma = 2.5$, (c) $\varsigma = 5.3$, (d) $\varsigma = 3.518$, (e) $\varsigma = 4.13$, (f) $\varsigma = 4.17$, (g) $\varsigma = 4.2$, (h) $\varsigma = 4.5$, and (i) $\varsigma = 4.8$.

slightly vary for different weak effects. To illustrate the typical variation of m and ς and the resulting bifurcation diagram, we utilize the same parameter values as in Fig. 24 and present the results in Fig. 14. The emergence of the Neimark–Sacker bifurcation, which ultimately leads to chaos, is evident in Figs. 26(i) and 27(l).

Furthermore, to investigate the sensitivity of the bifurcation diagrams shown in Figs. 26(i) and 27(l) to initial conditions, we choose the initial points (0.4,0.41) and (0.4,0.4), respectively, as depicted in Figs. 15(a) and 15(b). As a result, even slight variations in the initial population densities lead to different outcomes, underscoring the significance of meticulously selecting initial values in numerical simulations to capture the system's behavior faithfully. The presented bifurcation analysis offers valuable insights into the system's dynamics and can aid in predicting and controlling its behavior under diverse conditions.

VI. NUMERICAL SIMULATION AND ANALYSIS

In this section, we present a detailed analysis of the parameter values and equilibrium of the system (1.2).

(1) Based on Theorems 6 and 7, appropriate parameters were selected to showcase the existence and stability of the equilibrium point of system (1.2). It is worth mentioning that

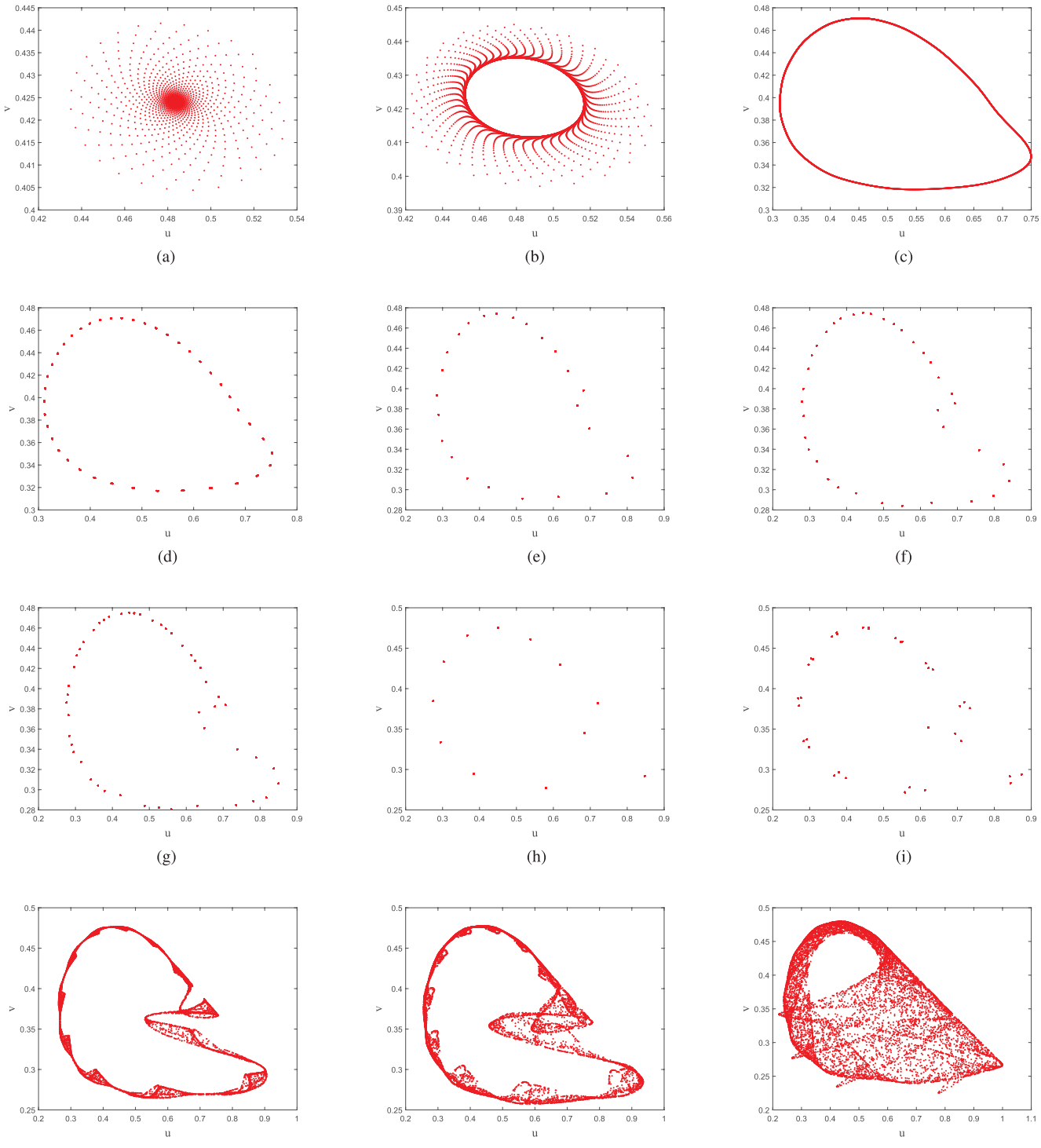

FIG. 27. Phase diagrams corresponding to Figs. 24(c) and 24(d). (a) $\varsigma = 1.3$, (b) $\varsigma = 1.47$, (c) $\varsigma = 3$, (d) $\varsigma = 3.03$, (e) $\varsigma = 3.365$, (f) $\varsigma = 3.691$, (g) $\varsigma = 3.753$, (h) $\varsigma = 3.868$, (i) $\varsigma = 3.913$, (j) $\varsigma = 4$, (k) $\varsigma = 4.1$, and (l) $\varsigma = 4.35$.

the existence of E_1 is strongly affected by the value of m. In particular, E_1 does not exist when m is weak; instead, E_0 becomes a saddle point. Specifically, the selection of the system parameters for Fig. 1 included $h = 0.9$, $e = 0.2$, $d = 0.2$, $a = 0.8$, $k = 0.2$, $b = 0.3$, and $m = -0.3$. This system has only two equilibrium points, E_0 and E_2, where E_2 is globally asymptotically stable. Therefore, any trajectory starting from a point close to E_2 will converge to E_2 over time. In Fig. 2, the same parameter values were selected as in Fig. 1, except $d = 0.1$. In this case, system (1.2) exhibits three equilibrium points: E_0, E_2, and E_3. Notably, E_2 becomes a saddle point, whereas E_3 becomes a globally asymptotically stable node. As a result, any trajectory originating from a point close to E_3 will eventually converge to E_3 over time. Furthermore, the system in Fig. 3 is characterized by parameter values of $h = 0.2$, $e = 0.1$, $d = 0.5$, $a = 0.8$, $k = 0.1$, $b = 0.6$, and $m = -0.3$. This system possesses three equilibria: E_0, E_2, and E_3. Of these, E_0 and E_2 are saddle points, while E_3 is a globally asymptotically stable focal point. In the long run, any trajectory beginning near E_3 will spiral inward toward E_3. Finally, Fig. 4 displays the simulation results for system (1.2) with the same parameter values as in Fig. 3, except $d = 0.1$ and $b = 0.4$. This scenario is significant as the coexisting equilibrium point E_3 is the instability focus, and a stable limit cycle emerges close to E_3, to which all trajectories beginning from any point ultimately converge. These findings offer further support for the theoretical results and underscore the critical role of parameter values in determining the stability and dynamics of the system.

(2) Based on Theorems 6 and 7, system (1.2) undergoes a qualitative change as the strength of the Allee effect increases. Specifically, as m approaches the strong Allee effect, system (1.2) exhibits a saddle point E_1, whereas E_0 remains locally asymptotically stable. The isotropic line of E_1 divides the plane into two regions, where the initial point on the left is attracted to E_0. In contrast, the initial point on the right enters the locally asymptotically stable coexistence equilibrium $E_3(0.951\,763, 0.024\,165\,9)$. In Figs. 5–8, the equilibrium point E_2 acts as the saddle point, while in Fig. 9, E_2 is locally asymptotically stable. Figure 5 represents system (1.2) with the same parameters as Fig. 3, except that $m = 0.6$. In Fig. 6, the parameters of the system (1.2) are $h = 0.8, e = 0.1, d = 0.3, a = 0.8, k = 0.1, b = 0.6, m = 0.04$, and the coexistence equilibrium $E_3(0.654\,838, 0.336\,124)$ becomes a stable focus. In Fig. 7, system (1.2) has the same parameters as in Fig. 1, except that $d = 0.1, m = 0.04$, and the coexisting equilibrium point $E_3(0.470\,783, 0.15)$ is an unstable source. In Fig. 8, system (1.2) has parameters $h = 0.8$, $e = 0.1$, $d = 0.3$, $a = 0.8$, $k = 0.1$, $b = 0.6$, $m = 0.3$, and the coexisting equilibrium point $E_3(0.654\,838, 0.196\,639)$ becomes the focus of instability, resulting in a stable limit cycle around $E_3(0.654\,838, 0.196\,639)$. The isotropic line of E_1 divides the plane region into orbits, some drawn into the limit cycle and some into E_0. In Fig. 9, system (1.2) has parameters $h = 0.5$, $e = 0.1$, $d = 0.5$, $a = 0.8$, $k = 0.1$, $b = 0.3$, $m = 0.3$, and the coexisting equilibrium point E_3 (1.2) does not exist. In contrast, the boundary equilibrium point E_2 is locally stable. The isotropic lines of E_1 divide the orbit in the plane region, with part of it being attracted by E_0 and the rest entering E_2.

(3) Theorem 9 states that if $J_{11}(x_3, y_3) > 0$ and $T^2 - 4D < 0$, then system (1.2) generates a Hopf bifurcation around the equilibrium point E_3 at m. In Fig. 10, we consider system (1.2) with parameter values $h = 0.5, e = 0.1, d = 0.25, a = 0.8$, $k = 0.1, b = 0.56$, which yields $m^* = -0.25$. Subfigures (a) and (b) depict the bifurcation diagrams concerning the parameter m with $q = 0.98$. The equilibrium point analysis reveals that E_0 is a saddle point, and E_1 does not exist when m exhibits a weak Allee effect. In contrast, when m exhibits a strong Allee effect, E_0 is locally stable, and E_1 is a saddle point. In subfigures (c) and (d), we set $m = -0.15$ satisfying $m < m^*$. System (1.2) has an unstable coexistence equilibrium $E_3(0.484, 0.422)$ and a limit cycle. In subfigures (e) and (f), $m = 0$ satisfying $m > m^*$. The system (1.2) has an unstable coexistence equilibrium E_3 $(0.484, 0.325)$, at which point the limit cycle expands. Therefore, any trajectory from any point in the plane will be attracted to the limit cycle, for example, the initial point (1,0.6). Finally, in subfigures (g) and (h), we consider $m = 0.15$ satisfying $m > m^*$. System (1.2) has an unstable coexistence equilibrium $E_3(0.484, 0.292)$. Since m exhibits a strong Allee effect, the boundary equilibrium point $E_1(0.004, 0)$ appears to be the saddle point, and E_0 is locally stable. The trajectory from the initial point (1,0.6) reaches the stable point E_0 through E_1.

(4) System (1.2) is affected by the strength of the Allee effect producing different Hopf bifurcations around E_3 with parameters b. In Fig. 11, the parameters of system (1.2) have values $h = 0.5, d = 0.25, a = 0.8, k = 0.1, m = -0.3, q = 0.98$, and the Hopf bifurcation value of b is $b^* = 0.57$. Subfigures (a) and (b) are bifurcation diagrams concerning the parameter b with $m = -0.3, q = 0.98$. By Theorem 6, system (1.2) has two equilibria E_0 and E_1 as saddle points, and one coexisting equilibrium E_3, and E_3 is globally stable when $b < b^*$. In subfigures (c) and (d), the value of b takes 0.6, satisfying $b > b^*$. System (1.2) has an unstable coexistence equilibrium $E_3(0.438, 0.518)$ and a stable limit cycle. The limit cycle will attract trajectories from (0.001,0.6) and (1,0.6). Note that the limit cycle expands as b increases. In Fig. 12, system (1.2) picks the same parameters as in Fig. 11, except that $m = 0.04$, then the Hopf bifurcation value of b is $b^* = 0.465$. Subfigures (a) and (b) are bifurcation diagrams concerning the parameter b with $m = 0.04, q = 0.98$. The system is locally asymptotically stable at its equilibrium point E_0 and produces a boundary equilibrium point $E_1(m, 0)$ that is a saddle point. When $b < b^*$, E_3 is globally stable. In subfigures (c) and (d), the value of b takes 0.5 and satisfies $b > b^*$. System (1.2) has an unstable coexistence equilibrium $E_3(0.556, 0.309)$ and a stable limit cycle. Trajectories from (0.001,0.6) and (0.04,0.001) will be attracted by E_0. Trajectories from (1,0.6) and (0.041,0.001) reach the limit cycle quickly. In subfigures (e) and (f), the value of b is taken to be 0.6, and system (1.2) has an unstable coexistence equilibrium $E_3(0.438, 0.299)$ and a stable limit cycle. Trajectories from (0.001,0.6), (0.04,0.001) and (1,0.6) will be attracted by E_0. The track from (0.041,0.001) passes through the saddle point E_2 in sufficient time to reach the limit cycle. Note that the limit cycle expands as b increases.

(5) The analysis of the parameters d, e, h is similar to that of b. We give a brief description. (i) In Fig. 16, system (1.2) has

parameter values $h = 0.5$, $b = 0.5$, $a = 4/5$, $k = 0.2$, $e = 0.1$, $m = -0.3$, $q = 0.98$ and the Hopf bifurcation value of d is $d^* = 0.235$. Subfigures (a) and (b) are bifurcation diagrams with respect to parameters d, $m = -0.3, q = 0.98$. In subfigures (c) and (d), $d = 0.2$ satisfying $d < d^*$. System (1.2) has an unstable coexistence equilibrium $E_3(0.415, 0.516)$ and a stable limit cycle. The limit cycle will attract trajectories from (0.001,0.6) and (1,0.6). In Fig. 17, system (1.2) is chosen with the same parameters as in Fig. 16, except that $m = 0.04$, then the Hopf bifurcation value of d is $d^* = 0.275$. Subfigures (a) and (b) are bifurcation diagrams concerning the parameter d, where $m = 0.04$ and $q = 0.98$. In subfigures (c) and (d), $d = 0.2$ satisfying $d < d^*$. System (1.2) has an unstable coexistence equilibrium $E_3(0.415, 0.277)$ and a stable limit cycle. Trajectories from (0.001,0.6) and (1,0.6) will be attracted to E_0. Trajectories from (0.041,0.001) reach the limit cycle quickly. In subfigures (e) and (f), the value of d is 0.25, and system (1.2) has an unstable coexistence equilibrium $E_3(0.556, 0.309)$ and a stable limit cycle. Trajectories from (0.001,0.6) and (0.04,0.0001) will be attracted by E_0. The trajectory from (1,0.6) passes the saddle point E_2 in enough time to reach the limit cycle. (ii) In Fig. 18, system (1.2) has parameter values $h = 0.5$, $d = 1/4$, $a = 4/5$, $k = 0.1$, $b = 0.5$, $m = -0.05$, $q = 0.98$ and the Hopf bifurcation value of e is $e^* = 0.18$. Subfigures (a) and (b) are bifurcation diagrams for the parameters e with $m = -0.05, q = 0.98$. In subfigures (c) and (d), $e = 0$ satisfying $e < e^*$. System (1.2) has an unstable coexistence equilibrium $E_3(0.373, 0.292)$ and a stable limit cycle. The limit cycle will attract trajectories from (1,0.6). In Fig. 19, system (1.2) picks the same parameters as in Fig. 18, except that $m = 0.04$, then the Hopf bifurcation value of e is $e^{**} = 0.22$. Subfigures (a) and (b) are bifurcation diagrams for the parameter d, where $m = 0.04$ and $q = 0.98$. In subfigures (c) and (d), $e = 0$ satisfying $e < e^*$. System (1.2) has an unstable coexistence equilibrium $E_3(0.373, 0.233)$ and a stable limit cycle. Trajectories from (0.001,0.6) and (1,0.6) will be attracted to E_0. Trajectories from (0.041,0.001) reach the limit cycle quickly. In subfigures (e) and (f), the value of e is 0.05, and system (1.2) has an unstable coexistence equilibrium $E_3(393, 0.251)$ and a stable limit cycle. Trajectories from (0.001,0.6) and (0.04,0.0001) will be attracted by E_0. The trajectory from (1,0.6) passes the saddle point E_2 in enough time to reach the limit cycle. (iii) In Fig. 20, system (1.2) has parameter values $e = 0.1$, $d = 1/4$, $a = 4/5$, $k = 0.1$, $b = 0.5$, $m = -0.3$, $q = 0.98$ and the Hopf bifurcation value of h is $h^* = 0.43$. Subfigures (a) and (b) are bifurcation diagrams for the parameters h with $m = -0.3, q = 0.98$. In subfigures (c) and (d), $h = 0.35$ satisfying $h < h^*$. System (1.2) has an unstable coexistence equilibrium $E_3(0.429, 0.474)$ and a stable limit cycle. The limit cycle will attract trajectories from (0.001,0.6) and (1,0.6). In Fig. 21, system (1.2) has the same parameters as in Fig. 20, except that $m = 0.04$, then the Hopf bifurcation value of h is $h^* = 0.89$. Subfigures (a) and (b) are bifurcation diagrams for the parameter h, where $m = 0.04$ and $q = 0.98$. In subfigures (c) and (d), $h = 0.4$ satisfying $h < h^*$. The system (1.2) has an unstable coexistence equilibrium $E_3(0.448, 0.273)$ and a stable limit cycle. Trajectories from (0.001,0.6) and (1, 0.6) will be attracted to E_0. Trajectories from (0.041,0.001) reach the limit cycle quickly. In subfigures (e) and (f), the value of h is 0.6, and system (1.2) has an unstable coexistence equilibrium $E_3(0.516, 0.319)$ and a stable limit cycle. Trajectories from (0.001,0.6) and (0.04,0.0001) will be attracted by E_0. The trajectory from (0.041,0.001) and (1,0.6) passes the saddle point E_2 in enough time to reach the limit cycle.

(6) By Theorem 9, the dynamical system described by system (1.2) experiences a Hopf bifurcation around point E_3 when the parameter q reaches the critical value q^*. The influence of the Allee effect on this system is explored in Figs. 22 and 23, which demonstrate the bifurcation behavior at two different values of the parameter m, namely, $m = 0.04$ and $m = -0.3$, respectively. In Fig. 22, the system parameters are $h = 0.5$, $e = 0.1$, $b = 0.5556$, $a = 0.8$, $k = 0.2$, $b = 0.25$, and $m = 0.04$. The critical value of q is determined to be $q^* = 0.865$. Bifurcation diagrams for the parameter q are shown in subfigures (a) and (b). In subfigures (c) and (d), $q = 0.91$ satisfying $q < q^*$. The system possesses a locally stable equilibrium point E_0, two saddle points E_1 and E_2, and an unstable coexisting equilibrium point E_3 located at the coordinates (0.4837,0.5168). Trajectories originating from the initial points (0.17,0.5) converge toward E_0, while trajectories starting from (0.2,0.5) and (0.3,0.5) pass through E_2 and are attracted to the limit cycle. Analogously, in subfigures (c) and (d), the value of q is 0.95, and system (1.2) has an unstable coexistence equilibrium $E_3(0.483\,47, 0.290\,747)$ and a stable limit cycle. Trajectories from (0.17,0.5) and (0.2,0.5) will be attracted by E_0. The trajectory from (0.3,0.5) passes the saddle point E_2 in enough time to reach the limit cycle. Figure 23 uses the same system parameters as in Fig. 22, except that $m = -0.3$ is chosen instead of $m = 0.04$. The critical value of q is found to be $q^* = 0.85$. Bifurcation diagrams for q are shown in subfigures (a) and (b), while subfigures (c) and (d) depict the dynamics of the system when q is set to 0.95. In this case, the system lacks the equilibrium point E_1 and possesses a locally stable equilibrium point E_0, a saddle point E_2, and an unstable coexisting equilibrium point E_3 situated at the coordinates (0.2564,0.4506). The trajectory originating from (0.0001,0.6) passes through E_0, E_2 and is attracted to the limit cycle, while the trajectory from (0.2564,0.4506) is also drawn toward the limit cycle.

(7) system (1.2) generates Neimark–Sacker bifurcation at weak Allee effects with bifurcation parameters of ς. In Figs. 24(a) and 24(b), system (1.2) has parameter values $h = 0.5$, $e = 0.1$, $b = 0.556$, $a = 4/5$, $k = 0.5$, $m = -0.5$, $q = 0.98$, $d = 0.095$ and the initial point is (0.5,0.3). By Theorem 12, E_0 is a saddle point, E_2 is locally unstable, and E_3 is unstable at $\varsigma^* = 2.45$. In Figs. 24(c) and 24(d), system (1.2) has the same parameter values as in Figs. 24(a) and 24(b), except that $m = -0.35$ and the initial point is (0.4,0.41). By simple calculation, E_0 is the saddle point, E_2 is the saddle point, and E_3 is unstable at $\varsigma^* = 1.44$. We compare subfigures (a) and (b) as well as (c) and (d), and it is clear that subfigures (c) and (d) have a more complex period window. Figure 25 shows a detailed plot of Figs. 24(c) and 24(d) at (3.5,4). System (1.2) appears to have several cycle windows in (3.5,4), including periodic-25 and 40 orbits, demonstrating the complex behavior of system (1.2).

Figure 26 is the corresponding phase diagram of Figs. 24(a) and 24(b), showing the evolution of the dynamical behavior of ς at $m = -0.5$. At $\varsigma = 2.4$ (a), E_3 is the stable focus; as ς crosses the bifurcation point to reach 2.5 (b), E_3 becomes unstable, and a stable invariant cycle appears; as ς increases, the constant cycle begins to expand, e.g., $\varsigma = 3$ (c) and $\varsigma = 3.518$ (d); as $\varsigma = 4.13$ (e), system (1.2) emerges with periodic-9 orbits; at $\varsigma = 4.17$ (f), each period point begins to expand into a small cycle of periods; until $\varsigma = 4.5$ (g), the system begins to enter a chaotic state, and at $\varsigma = 4.8$, it enters a fully chaotic state.

Figure 27 is the corresponding phase diagram of Figs. 24(c) and 24(d), showing the evolution of the dynamical behavior of ς at $m = -0.35$. At $\varsigma = 1.3$ (a), E_3 is the stable focus; as ς crosses the bifurcation point to reach 1.47 (b), E_3 becomes unstable, and a stable invariant cycle appears; as ς increases, the constant cycle begins to expand, e.g., $\varsigma = 3$ (c); as $\varsigma = 3.03$ (d), 3.65 (e), 3.691 (f), 3.753 (g), 3.868 (h), 3.913 (i) the system appears to have periodic-40, 25, 40, 51, 12, 36 orbits, respectively; $\varsigma = 4$ (j), 4.1 (k), system (1.2) begins to overstep into the chaotic state and enters it ultimately at $\varsigma = 4.35$ (l).

VII. CONCLUSION

This paper provides insight into the effects of Allee and fear effects in a disordered prey–predator system with group defense and prey refuge. The work demonstrates the existence, uniqueness, non-negativity, and boundedness of the system's solution, which are fundamental properties in dynamical systems theory. Furthermore, the coexistence and stability of the equilibrium of system (1.2) are thoroughly analyzed. In particular, the paper studies the coexistence equilibrium with respect to the occurrence of Hopf bifurcations at five crucial parameters and the memory effects q. Additionally, system (1.2) is discretized, and the impact of step size on the stability and bifurcation of the system is investigated. Our findings reveal the process from stability to chaos, providing important insights into the dynamics of the system. The following conclusions are obtained:

(1) The Allee effect plays a pivotal role in determining the persistence and stability of a system. When the effect is strong, system (1.2) exhibits a locally asymptotically stable extinction equilibrium point E_0 and a saddle point E_1. The isoclinic line associated with E_1 divides the initial population density into two distinct regions. If the initial density is near E_0, the system population is at risk of extinction. Conversely, suppose the initial density falls within the other region. In that case, four scenarios may arise: predator extinction and prey flourishing without a coexistence equilibrium, population coexistence, cyclic behavior of the two populations, or complete extinction of the system's population. When the Allee effect weakens, the boundary equilibrium point E_1 collides with the extinction equilibrium point E_0 to form a single saddle point. Consequently, only one extinction equilibrium point exists. After a prolonged period, the initial density of the two populations will lead to one of three scenarios: predator extinction and prey flourishing in the absence of a coexistence equilibrium, population coexistence, two populations entering a periodic state.

(2) In the presence of a coexistence equilibrium in the system, we investigate the occurrence of a Hopf bifurcation of the system at E_3. Specifically, we show that if the initial densities of two species are not in the attraction domain of the extinction equilibrium point, then it is possible to reduce the Allee effect, conversion rate of the prey, amount of the prey available to the predator and memory effect or increase threshold for the transition between herd grouping and solitary behavior, and death rate of the predator population, eliminating the limit cycle and allowing the system to reach stable coexistence. This has significant implications for the ecosystem as a whole. By achieving stable coexistence, predator populations can acquire their biomass over a more extended period, which is crucial for survival. In addition, the increase in prey group behavior has a protective effect on the predator population, contributing to the stability and persistence of the entire ecosystem.

(3) The Allee effect plays a pivotal role in determining the persistence of fractional-order systems (1.2) in prey–predator ecological systems, enabling the prey species to acquire experience and memory from past encounters, thereby altering their behavior. This high memory capacity represents a crucial characteristic that needs to be considered when simulating the dynamics of such ecological systems. Moreover, the choice of step size in modeling fractional-order systems can significantly impact numerical simulations and provide a comprehensive understanding of the dynamics, especially regarding bifurcation to chaos. For instance, in the context of the stability of discrete systems and the creation of a Neimark–Sacker bifurcation at E_3, selecting the appropriate step size is essential to maintain stability in both populations, consistent with the continuous case. However, if the step size exceeds a certain threshold, the stability of the discrete system can undergo dramatic changes, leading to multi-periods and chaos. Therefore, it is crucial to consider the order and step size when the dynamics of a prey–predator ecosystem.

The importance of our results for the accurate modeling and analysis of ecosystems is significant. By considering the order and step length of the discrete system, we can gain a more comprehensive understanding of the underlying dynamics of prey–predator interactions. It also provides information for developing effective ecological conservation management strategies to help ensure these complex ecosystems' long-term stability and sustainability. Inspired by stability analysis and chaotic attractors, our future work will focus on bistability phenomena in systems and more complex dynamical phenomena, such as co-dimensional bifurcation, chaotic synchronization, and control, which will also be investigated.

ACKNOWLEDGMENTS

The authors are grateful to the referees for their useful suggestions that have significantly improved the article. The authors appreciate the help of the editor. This research was supported by the National Natural Science Foundation of China (NNSFC) (Grant Nos. 12101608, 62103422, and 12301325).

AUTHOR DECLARATIONS

Conflict of Interest

The authors have no conflicts to disclose.

Author Contributions

Wenhui Tan: Conceptualization (equal). **Hao Tian:** Writing – review & editing (equal). **Yanjie Song:** Writing – review & editing (equal). **Xiaojun Duan:** Writing – review & editing (equal).

DATA AVAILABILITY

The data that support the findings of this study are available from the corresponding author upon reasonable request.

REFERENCES

[1]S. K. Sasmal, "Population dynamics with multiple Allee effects induced by fear factors—A mathematical study on prey-predator interactions," Appl. Math. Model. **64**, 1–14 (2018).
[2]S. Sajan, S. K. Sasmal, and B. Dubey, "A phytoplankton-zooplankton-fish model with chaos control: In the presence of fear effect and an additional food," Chaos **32**, 013114 (2022).
[3]K. B. Blyuss, S. N. Kyrychko, and Y. N. Kyrychko, "Time-delayed and stochastic effects in a predator-prey model with ratio dependence and Holling type III functional response," Chaos **31**, 073141 (2021).
[4]J. Lotka, "Analytical note on certain rhythmic relations in organic systems," Proc. Natl. Acad. Sci. U.S.A. **6**, 410–415 (1920).
[5]V. Volterra, *Variazioni e fluttuazioni del numero d'individui in specie animali conviventi* (Societá anonima tipografica "Leonardo da Vinci," 1927).
[6]J. Alidousti and M. M. Ghahfarokhi, "Dynamical behavior of a fractional three-species food chain model," Nonlinear Dyn. **95**, 1841–1858 (2019).
[7]K. Sarkar and S. Khajanchi, "An eco-epidemiological model with the impact of fear," Chaos **32**, 083126 (2022).
[8]R. Yang, C. Nie, and D. Jin, "Spatiotemporal dynamics induced by nonlocal competition in a diffusive prey-predator system with habitat complexity," Nonlinear Dyn. **110**, 879–900 (2022).
[9]L. Zhang and S. Fu, "Global bifurcation for a Holling–Tanner predator-prey model with prey-taxis," Nonlinear Anal-Real. **47**, 460–472 (2019).
[10]C. Arancibia-Ibarra, M. Bode, J. Flores, G. Petter, and P. van Heijster, "Turing patterns in a diffusive Holling–Tanner predator-prey model with an alternative food source for the predator," Commun. Nonlinear Sci. **99**, 105802 (2021).
[11]C. Xiang, M. Lu, and J. Huang, "Degenerate Bogdanov-Takens bifurcation of codimension 4 in Holling-Tanner model with harvesting," J. Differ. Equ. **314**, 370–417 (2022).
[12]X. Zhang and Z. Liu, "Periodic oscillations in age-structured ratio-dependent predator-prey model with Michaelis–Menten type functional response," Physica D **389**, 51–63 (2019).
[13]H. Chen and C. Zhang, "Dynamic analysis of a Leslie–Gower-type predator-prey system with the fear effect and ratio-dependent Holling III functional response," Nonlinear Anal-Model. **27**, 904–926 (2022).
[14]F. Wei and Q. Fu, "Hopf bifurcation and stability for predator-prey systems with Beddington-DeAngelis type functional response and stage structure for prey incorporating refuge," Appl. Math. Model. **40**, 126–134 (2016).
[15]S. Sarwardi, M. M. Haque, and S. Hossain, "Analysis of Bogdanov–Takens bifurcations in a spatiotemporal harvested-predator and prey system with Beddington-DeAngelis-type response function," Nonlinear Dyn. **100**, 1755–1778 (2020).
[16]J. P. Tripathi, D. Jana, and V. Tiwari, "A Beddington-DeAngelis type one-predator two-prey competitive system with help," Nonlinear Dyn. **94**, 553–573 (2018).
[17]Y. Liu and J. Wei, "Double Hopf bifurcation of a diffusive predator-prey system with strong Allee effect and two delays," Nonlinear Anal-Model. **26**, 72–92 (2021).
[18]Z. Bi, S. Liu, and M. Ouyang, "Spatial dynamics of a fractional predator-prey system with time delay and Allee effect," Chaos Soliton. Fract. **162**, 112434 (2022).
[19]P. A. Naik, Z. Eskandari, M. Yavuz, and J. Zu, "Complex dynamics of a discrete-time Bazykin–Berezovskaya prey-predator model with a strong Allee effect," J. Comput. Appl. Math. **413**, 114401 (2022).
[20]X. Wang, L. Zanette, and X. Zou, "Modelling the fear effect in predator-prey interactions," J. Math. Biol. **73**, 1179–1204 (2016).
[21]P. K. Tiwari, K. A. N. A. Amri, S. Samanta, Q. J. A. Khan, and J. Chattopadhyay, "A systematic study of autonomous and nonautonomous predator-prey models with combined effects of fear, migration and switching," Nonlinear Dyn. **103**, 2125–2162 (2021).
[22]S. Mondal and G. P. Samanta, "Impact of fear on a predator-prey system with prey-dependent search rate in deterministic and stochastic environment," Nonlinear Dyn. **104**, 2931–2959 (2021).
[23]R. Yang, C. Nie, and D. Jin, "Spatiotemporal dynamics induced by nonlocal competition in a diffusive predator-prey system with habitat complexity," Nonlinear Dyn. **110**, 879–900 (2022).
[24]D. Geng, W. Jiang, Y. Lou, and H. Wang, "Spatiotemporal patterns in a diffusive predator-prey system with nonlocal intraspecific prey competition," Stud. Appl. Math. **148**, 396–432 (2022).
[25]D. Geng and H. Wang, "Normal form formulations of double-Hopf bifurcation for partial functional differential equations with nonlocal effect," J. Differ. Equ. **309**, 741–785 (2022).
[26]Y. Sekerci and S. Petrovskii, "Mathematical modelling of plankton-oxygen dynamics under the climate change," B. Math. Biol. **77**, 2325–2353 (2015).
[27]Y. Kuang and Y. Takeuchi, "Predator-prey dynamics in models of prey dispersal in two-patch environments," Math. Biosci. **120**, 77–98 (1994).
[28]S. R. J. Jang and J. Baglama, "A nutrient-prey-predator model with intratrophic predation," Appl. Math. Comput. **129**, 517–536 (2002).
[29]S. Djilali, "Pattern formation of a diffusive predator-prey model with herd behavior and nonlocal prey competition," Math. Method Appl. Sci. **43**, 2233–2250 (2020).
[30]W. Yang, "Analysis on existence of bifurcation solutions for a predator-prey model with herd behavior," Appl. Math. Model. **53**, 433–446 (2018).
[31]S. Yuan, C. Xu, and T. Zhang, "Spatial dynamics in a predator-prey model with herd behavior," Chaos **23**, 033102 (2013).
[32]V. Ajraldi, M. Pittavino, and E. Venturino, "Modeling herd behavior in population systems," Nonlinear Anal-Real. **12**, 2319–2338 (2011).
[33]Y. Lv, "Turing-Hopf bifurcation in the predator-prey model with cross-diffusion considering two different prey behaviours transition," Nonlinear Dyn. **107**, 1357–1381 (2022).
[34]J. N. McNair, "Stability effects of prey refuges with entry-exit dynamics," J. Theor. Biol. **125**, 449–464 (1987).
[35]D. Mukherjee, "The effect of prey refuges on a three species food chain model," Differ. Equ. Dyn. Syst. **22**, 413–426 (2014).
[36]J. Alidousti and M. M. Ghahfarokhi, "Stability and bifurcation for time delay fractional predator-prey system by incorporating the dispersal of prey," Appl. Math. Model. **72**, 385–402 (2019).
[37]N. Zhang, Y. Kao, and B. Xie, "Impact of fear effect and prey refuge on a fractional order prey-predator system with Beddington-DeAngelis functional response," Chaos **32**, 043125 (2022).
[38]S. Dey, S. Ghorai, and M. Banerjee, "Analytical detection of stationary and dynamic patterns in a prey-predator model with reproductive Allee effect in prey growth," arXiv:2302.02582 (2023).
[39]R. Han and B. Dai, "Spatiotemporal pattern formation and selection induced by nonlinear cross-diffusion in a toxic-phytoplankton–zooplankton model with Allee effect," Nonlinear Anal-Real. **45**, 822–853 (2019).
[40]D. Sen, S. Ghorai, S. Sharma, and M. Banerjee, "Allee effect in prey's growth reduces the dynamical complexity in prey-predator model with generalist predator," Appl. Math. Model. **91**, 768–790 (2021).
[41]S. Rana, A. R. Bhowmick, and T. Sardar, "Invasive dynamics for a predator-prey system with Allee effect in both populations and a special emphasis on predator mortality," Chaos **31**, 033150 (2021).
[42]A. W. Stoner and M. Ray-Culp, "Evidence for Allee effects in an over-harvested marine gastropod: Density-dependent mating and egg production," Mar. Ecol. Prog. Ser. **202**, 97–302 (2000).
[43]A. M. Kramer, B. Dennis, A. M. Liebhold, and J. M. Drake, "The evidence for Allee effects," Popul. Ecol. **51**, 341–354 (2009).

[44]L. Berec, E. Angulo, and F. Courchamp, "Multiple Allee effects and population management," Trends Ecol. Evol. **22**, 185–191 (2007).
[45]R. Han, S. Dey, and M. Banerjee, "Spatio-temporal pattern selection in a prey-predator model with hunting cooperation and Allee effect in prey," Chaos Soliton. Fract. **171**, 113441 (2023).
[46]B. Xie and Z. Zhang, "Impact of Allee and fear effects in a fractional order prey-predator system incorporating prey refuge," Chaos **33**, 013131 (2023).
[47]J. Alidousti and M. M. Ghahfarokhi, "Stability and bifurcation for time delay fractional predator prey system by incorporating the dispersal of prey," Appl. Math. Model. **72**, 85–402 (2019).
[48]E. Bonyah, A. Atangana, and A. A. Elsadany, "A fractional model for predator-prey with omnivore," Chaos **29**, 013136 (2019).
[49]B. S. T. Alkahtani, "Analytical study of the complexities in a three species food web model with modified Caputo-Fabrizio operator," Fract. Fraction. **7**, 105 (2023).
[50]K. Diethelm, *The Analysis of Fractional Differential Equations: An Application Oriented Exposition Using Differential Operators of Caputo Type* (Springer Science & Business Media, 2010).
[51]Z. M. Odibat and N. T. Shawagfeh, "Generalized Taylor's formula," Appl. Math. Comput. **186**, 286–293 (2007).
[52]S. Liang, R. Wu, and L. Chen, "Laplace transform of fractional order differential equations," Electron. J. Differ. Equ. **139**, 1–15 (2015).
[53]L. Kexue and P. Jigen, "Laplace transform and fractional differential equations," Appl. Math. Lett. **24**, 2019–2023 (2011).
[54]I. Petrá, *Fractional-Order Nonlinear Systems: Modeling, Analysis and Simulation* (Springer Science & Business Media, 2011).
[55]Y. A. Kuznetsov, I. A. Kuznetsov, and Y. Kuznetsov, *Elements of Applied Bifurcation Theory* (Springer, New York, 2004).
[56]L. Yuan and Q. Yang, "Bifurcation, invariant curve and hybrid control in a discrete-time predator-prey system," Appl. Math. Model. **39**, 2345–2362 (2015).
[57]A. M. A. ElSayed and S. M. Salman, "On a discretization process of fractional-order Riccati differential equation," J. Fract. Calc. Appl. **4**, 251–259 (2013).